

Delft University of Technology
Master's Thesis in Sustainable Energy Technologies

Algorithm for Determining the Hosting Capacity of Independent PV, or EV Charger Systems.

In Industrial and Commercial LV Networks, with Respect to Slow Voltage Variations and Voltage Unbalances.

J. L. Christiaanse

Algorithm for Determining the Hosting Capacity of
Independent PV, or EV Charger Systems.
In Industrial and Commercial LV Networks, with
Respect to Slow Voltage Variations and Voltage
Unbalances.

Master's Thesis in Sustainable Energy Technologies

Faculty of Electrical Engineering, Mathematics and Computer Science
Delft University of Technology
Mekelweg 4, 2628 CD Delft, The Netherlands

J. L. Christiaanse
j.l.christiaanse@student.tudelft.nl

21st August 2019

Author

J. L. Christiaanse (j.l.christiaanse@student.tudelft.nl)

Title

Algorithm for Determining the Hosting Capacity of Independent PV,
or EV Charger Systems in Industrial and Commercial LV Networks,
with Respect to Slow Voltage Variations and Voltage Unbalances.

MSc presentation

30th of august 2019

Graduation Committee

Prof. Dr. Ir. J.F.G. Cobben TU Eindhoven, supervisor

Dr. Ir. S.H. Tindemans TU Delft

Prof. Dr. Ir. P. Vaessen TU Delft

Abstract

In this thesis, an algorithm that calculates the hosting capacity of independent PV, or EV charger systems was created. The hosting capacity is based on slow voltage variations and voltage unbalances caused by worst case PV generation and EV charging scenarios. The algorithm was run for four different commercial and industrial networks, and a range of network impedances. The outcome of the algorithm resulted into two figures for each of the networks, representing the possible installed capacity of PV and EV charger systems, respectively.

Contents

1	Introduction	1
1.1	Research Context	1
1.2	Research Question	2
1.3	Research Methodology	2
1.4	Thesis Structure	3
I	Theory	5
2	Slow Voltage Variations and Voltage Unbalances in LV networks	7
2.1	Slow Voltage Variations	7
2.1.1	Definition	7
2.1.2	Causes	7
2.1.3	Regulations	8
2.2	Voltage Unbalances	9
2.2.1	Definition	9
2.2.2	Causes	10
2.2.3	Regulations	10
2.3	Responsibilities	10
3	Slow Voltage Variations and Voltage Unbalances in PV and EV Charger Systems	13
3.1	PV System	13
3.1.1	Definition	13
3.1.2	Voltage Level	13
3.1.3	Voltage Unbalance	14
3.2	EV Charger Systems	15
3.2.1	Definition	15
3.2.2	Voltage Level and Unbalances	15

II	Ground Truth Data	17
4	PV System Data Analysis	19
4.1	Background	19
4.2	Goal	19
4.3	Configuration	20
4.3.1	Time Line	20
4.3.2	Data Extraction	22
4.3.3	Processing	23
4.4	Results	25
4.4.1	Apparent Power	25
4.4.2	Current Level	25
4.4.3	Current Unbalance	28
4.4.4	Voltage Level	30
4.4.5	Voltage Unbalance	32
4.5	PV System Behaviour	33
5	Electric Vehicle Chargers Data Analysis	35
5.1	Background	35
5.2	Goal	35
5.3	Set-Up	36
5.3.1	Configuration	36
5.3.2	Timeline	36
5.3.3	Data Extraction	36
5.4	Results	38
5.4.1	Apparent Power	38
5.4.2	Current Level	38
5.4.3	Current Unbalance	40
5.4.4	Voltage Level	41
5.4.5	Voltage Unbalance	42
5.5	EV Charging Behaviour	43
6	Network Data Analysis	45
6.1	Background	45
6.2	Goal	45
6.3	Set-Up	46
6.3.1	Configuration	46
6.3.2	Time Line	46
6.3.3	Data Extraction	46
6.3.4	Processing	47
6.4	Results and Behaviour	48
6.4.1	Impedances	48
6.4.2	Network N1	49
6.4.3	Network N2	52

6.4.4	Network N3	55
6.4.5	Network N4	58
6.5	Behaviour of the Networks	60
III Hosting Capacity Algorithm		61
7	Hosting Capacity	63
7.1	Algorithm	63
8	Scenario Models	67
8.1	PV System	67
8.1.1	PV Model	67
8.1.2	Model vs Reality	70
8.2	EV Charger System	71
8.2.1	EV Charger Model	71
8.2.2	Model vs Reality	73
8.3	Utility Voltage	74
8.3.1	Utility Voltage Model	74
8.3.2	Model vs. Reality	76
9	Scenarios	79
9.1	The Scenario Maker	79
9.2	Worst Case PV Subscenario	80
9.3	Worst Case EV Subscenario	82
9.4	Worst Case Network Subscenario	83
9.5	Worst Case Utility Voltage Subscenario	84
10	Core Model	85
10.1	Input and Outputs	85
10.2	Core Model Explanation	87
10.2.1	Present Situation	87
10.2.2	New Situation	88
10.3	Core Model Equations	89
10.3.1	Load-Flow Equations	89
10.3.2	Voltage Unbalance	92
10.3.3	Transformer Total Load	92
11	Limits	93
11.1	PV System	94
11.2	EV Charger System	95
11.3	Network	95

12 Outcome of the Algorithm	97
12.1 Background	97
12.2 Algorithm Input	97
12.2.1 Network Impedance and limits	97
12.2.2 Scenarios	97
12.2.3 PV or EV Charging System feeder impedance	102
12.2.4 Installed Capacity P	102
12.3 Algorithm Output	103
12.3.1 Network N1	103
12.3.2 Network N2	104
12.3.3 Network N3	105
12.3.4 Network N4	106
12.4 Discussion of the Algorithm's Results	106
IV Discussion, Conclusion, Recommendations and Future Work	109
13 Discussion	111
14 Conclusion	113
15 Recommendations and Future Work	115

Chapter 1

Introduction

1.1 Research Context

Climate change is a big factor in promoting technologies that support sustainable electricity production and travel. The last decade's carbon dioxide (CO₂) levels are the highest in millennia [1]. As a consequence, the European Union is making efforts to cut its CO₂ emissions by 80%-95% by 2050, and aims to spend at least 20% of the EU budget towards climate change related issues [2]. In the Netherlands, governmental financial support towards driving electric vehicles (EV) [3], is provided. Finally, government policies have played a large role in reducing the costs of Photovoltaic (PV) systems [4]. Due to the climate change awareness amongst governments, it is believed that sustainable technologies, which reduce CO₂ emissions, will increase in the future.

However, PV systems and EVs, which are sustainable technology advancements, may impede the Power Quality (PQ) of low voltage (LV) networks. PQ refers to the collection of the characteristics in voltage and current behaviour, with which you can analyze the total quality of power. PV and EV charger systems in LV networks impede the PQ by impacting the voltage level, and causing voltage unbalances [5] [6] [7]. The risks of impacting the PQ beyond the LV network's limits, affect the network's hosting capacity of PV and EV charger systems.

Good understanding of the LV network provides insight about the likelihood and severity of these risks, and finally the hosting capacity. Moreover, it is believed that network power monitoring can play a large role. Power monitoring presents knowledge about the network's occurring voltages and currents, which is generally used to ensure safety, and improve efficiency [8]. However, it may be worthwhile to use this same information, about the voltage and current, in determining the hosting capacity of PV and EV charger systems.

1.2 Research Question

The objective is to find the independent PV, or EV charger system hosting capacity of an analyzed industrial or commercial network based on slow voltage variations and voltage unbalances. Evidently, this leads to the following research question.

”How can an industrial and commercial distribution network’s hosting capacity of independent PV, or EV charger systems, be determined, based on monitoring data, slow voltage variations and voltage unbalances?”

The main research question is supported by the following sub-questions:

1. Which properties of PV and EV charger systems influence slow voltage variations and unbalances?
2. Which properties of the industrial and commercial distribution network influence the slow voltage variations and unbalances?
3. What are the power quality requirements of industrial and commercial distribution network, PV, and EV charger system?
4. How can the above be incorporated within a model or algorithm that provides the hosting capacity?

1.3 Research Methodology

The first step to finding the hosting capacity was to understand how slow voltage variations and voltage unbalances, arise in the LV network with independent PV or EV charger systems installed. In this research, this understanding had come from literature work, but also measurement and monitoring data. Based on this knowledge, the relevant characteristics and behaviours, that effect these PQ aspects, of PV and EV charger systems were determined.

The second step was to gather the information about the LV network, and also determine its relevant characteristics and behaviours. This was performed by analyzing the LV networks, of which certain information and power monitoring data had been provided by the company HyTEPS.

The third step was to identify the slow voltage variation, and voltage unbalance limits with respect to PV and EV charger systems, and the network.

The fourth step was to define a core model that predicts the slow voltage and voltage unbalances in the LV network with either PV or EV charger system installed. This was then incorporated within an algorithm that finds the maximum capacity of the PV or EV charger system, based on the limits given.

The chosen programming language for the algorithm was Python. Python is free to use, and an accessible programming language to many academics.

1.4 Thesis Structure

This thesis is split into several parts, containing individual chapters. In the first part, "Theory", the theory behind slow voltage variations and voltage unbalances, and how these arise in LV networks with PV and EV charger systems, is explained. Chapter 2 focuses on the definition of these PQ aspects, and their relation to the current. Chapter 3 shows how PV and EV charger systems affect the current.

The second part, "Ground Truth Data", contains the analysis of PV and EV charger systems, and the industrial and commercial networks' data, given by the company HyTEPS. The PV and EV charger system analyses, in Chapter 4 and 5, are used as the foundation for the general PV and EV charger behaviours. In Chapter 6, the behaviours of the industrial and commercial networks, are also analyzed. Finally, the characteristics and data of these networks are used directly in the final algorithm.

The third part, "Hosting Capacity Algorithm", contains the explanation and application of the algorithm that calculates the hosting capacity of independent PV, or EV systems. The framework of the algorithm is explained in Chapter 7. The algorithm requires constructed scenarios that represent a LV network situation where either PV, or EV charger systems have been installed. The construction of these scenarios are explained in Chapter 8 and 9. Additionally, the algorithm contains a core model, which is explained in Chapter 10. Finally, the algorithm requires slow voltage variations and voltage unbalance limits, which are defined in Chapter 11. The results of the algorithm with the network data from Chapter 6, are shown in Chapter 12.

The fourth part, "Discussion, Conclusion, Future work and Recommendation" contains the final thoughts about the research, and the proposed algorithm.

Part I
Theory

Chapter 2

Slow Voltage Variations and Voltage Unbalances in LV networks

2.1 Slow Voltage Variations

2.1.1 Definition

The slow voltage variations are the changes in the 10 minute average RMS voltage magnitudes [9]. One of the causes of slow voltage variations are the daily load patterns of customers [10].

2.1.2 Causes

Figure 2.1 shows the relation between the voltage at the load, the utility voltage and the transport losses. In the electric network, the transport losses result in a voltage drop, which causes the voltage at the load to decrease with respect to the utility voltage.

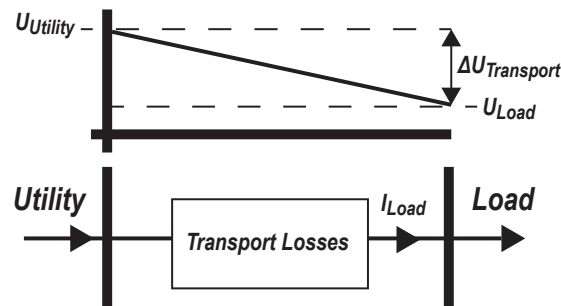


Figure 2.1: The voltage drop is the result of the transport losses, which occur in between the utility supply and the load.

This phenomena can be described in Equation 2.1. Here, U_{Load} , represents the load voltage in volts, the utility voltage, $U_{Utility}$, the transport impedance, $Z_{Transport}$, in ohms, and the load current, I_{Load} , in amps, which together represent the voltage drop $\Delta U_{Transport}$, in volts. The utility and load voltage and load current are phasors, whereas the voltage drop and impedance are complex numbers.

$$\bar{U}_{Load} = \bar{U}_{Utility} - \bar{I}_{Load} \cdot \bar{Z}_{Transport} = \bar{U}_{utility} - \Delta \bar{U}_{Transport} \quad (2.1)$$

One of the key characteristics of AC systems is the presence of active and reactive power in the network. The load demand can be a combination of both powers. Moreover, the reactive power can either be inductive, or capacitive. Depending on the resistive and reactive characteristics of the transport impedance, the load demand can result in a positive or negative voltage drop. For example, the active part and inductive part of a load will lead to a positive voltage drop, decreasing the RMS voltage at the load. However, the capacitive part of the load will lead to a negative voltage drop, increasing the RMS voltage at the load.

In LV networks, the network resistance is much greater than the reactance, meaning that the reactive power influence on the voltage drop is negligible. However, at the beginning of the LV network, directly behind the transformer, the reactive power can significantly influence the voltage drop due to the higher reactance to resistance (X/R) ratio of the transformer.

2.1.3 Regulations

There are regulations for the voltage levels in the LV network and the in-between voltage drop. The voltage in the LV network should not deviate more than 10% of the nominal voltage of 230 Volts [11]. Secondly, as illustrated in Figure 2.2, the IEC suggests a permissible voltage drop of 8% between the secondary side of the transformer and the final load, and 5% between the start of the installation and the final load.

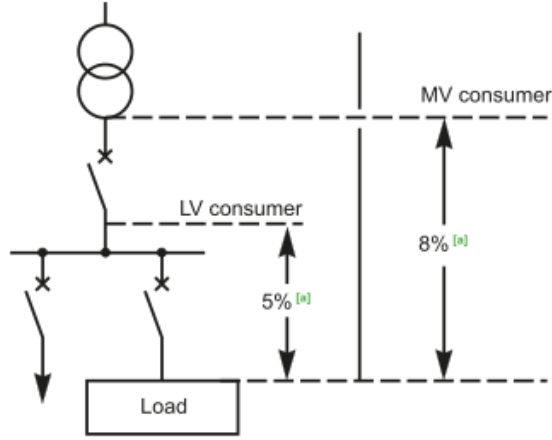


Figure 2.2: Maximum Voltage drop according to [a], the IEC60364-5-52. [12]

2.2 Voltage Unbalances

2.2.1 Definition

The definition of voltage unbalance, $\%VUF$, is defined as the ratio between the negative sequence, $V_{negative}$, and positive sequence, $V_{positive}$, component magnitude of the 10 minute average three-phase voltage [13], as shown in Equation 2.2.

$$\%VUF = \frac{V_{negative}}{V_{positive}} \cdot 100\% \quad (2.2)$$

The positive and negative sequence component are derived from the three-phase voltage, as described in Equations 2.3 and 2.4. Here, U_{L1} , U_{L2} , and U_{L3} are the line to neutral voltages.

$$\bar{V}_{positive} = \bar{U}_{L1} + a \cdot \bar{U}_{L2} + a^2 \cdot \bar{U}_{L3} \quad (2.3)$$

$$\bar{V}_{negative} = \bar{U}_{L1} + a^2 \cdot \bar{U}_{L2} + a \cdot \bar{U}_{L3} \quad (2.4)$$

Where, the definition of a and a^2 are the following:

$$a = 120^\circ \quad (2.5)$$

$$a^2 = 240^\circ \quad (2.6)$$

2.2.2 Causes

Voltage unbalances in the LV network arise due to unbalanced utility voltages, and/or unbalanced voltage drops between the phases. The latter are caused by unbalanced currents and/or unbalanced network impedances.

As an example, Figure 2.3 shows an unbalanced network where both loads are unequal, and no load is connected to the third phase. The unbalanced load lead to an unbalanced current, and a current flow in the neutral wire.

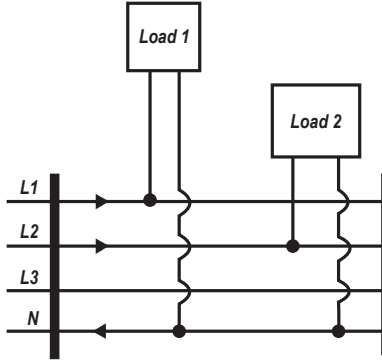


Figure 2.3: An unbalanced network where only the first two phases are loaded, and $Load_1 \neq Load_2$.

The voltage level in each phase can be described in Equation 2.7, where \bar{U}_{LxLoad} represent the phase voltage on the load. Indeed, Equation 2.7 is similar to Equation 2.1. However here, the voltage, current, and impedance differences between the individual phases are acknowledged as well.

For phase Lx in phases $L1$, $L2$, and $L3$:

$$\bar{U}_{LxLoad} = \bar{U}_{LxUtility} - \bar{I}_{LxLoad} \cdot \bar{Z}_{LxTransport} \quad (2.7)$$

2.2.3 Regulations

The IEC has provided limits for the voltage unbalance in the network. The 10 minute averages of the voltage unbalances, according to the definition, should not be more than 2% [14].

2.3 Responsibilities

Three main groups are involved with the voltage levels and voltage unbalances in the electric network. These groups are the device manufacturers, grid operators and customers.

The grid operator is responsible for the voltage at Point of Common Coupling (PCC). PCC is the point where the public grid ends, and the customer's network starts. Here, the slow voltage variations, and voltage unbalances must not exceed the limits as described in the Dutch regulations, NEN-EN 50160 [15].

The device manufacturer creates devices with a certain electromagnetic compatibility (EMC). This means that the device is compatible with certain levels of voltage magnitude, or voltage unbalances. The most commonly used international standards for the EMC are stated in the IEC 61000 series.

Finally, the customer is responsible for the current at PCC. The customer is allowed to draw as much current as stated per contract with the grid operator. By installing electric devices, the customer controls the current flow in the network. Therefore, to manage the current flow, the customer should design their network accordingly.

Chapter 3

Slow Voltage Variations and Voltage Unbalances in PV and EV Charger Systems

3.1 PV System

3.1.1 Definition

A PV system is a system that directly converts sunlight into electrical energy, which is then transformed into usable electricity for the intended load. The PV system contains a PV array, where light is converted in DC electricity, and an inverter, where the DC electricity is converted to AC electricity.

3.1.2 Voltage Level

As illustrated in Figure 3.1, the PV system injects current into the network. As described in Equation 3.1, the current, \bar{I}_{PV} , affects the voltage drop, $\Delta\bar{U}_{Transport}$, and finally the voltage level at the PV system, \bar{U}_{PV} . The same principle as described in section 2.1.2 is present. Here, due to the opposite direction of the current, the voltage drop leads to a voltage raise at the PV system.

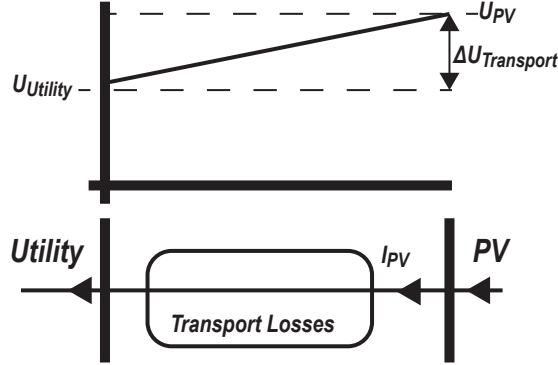


Figure 3.1: PV injection leads to a voltage raise at the PV system.

$$\bar{U}_{PV} = \bar{U}_{Utility} + \bar{I}_{PV} \cdot \bar{Z}_{Transport} = \bar{U}_{utility} + \Delta \bar{U}_{Transport} \quad (3.1)$$

As described in Figure 3.2, PV systems that are connected in the lower levels of the customer's network may affect the higher levels as well.

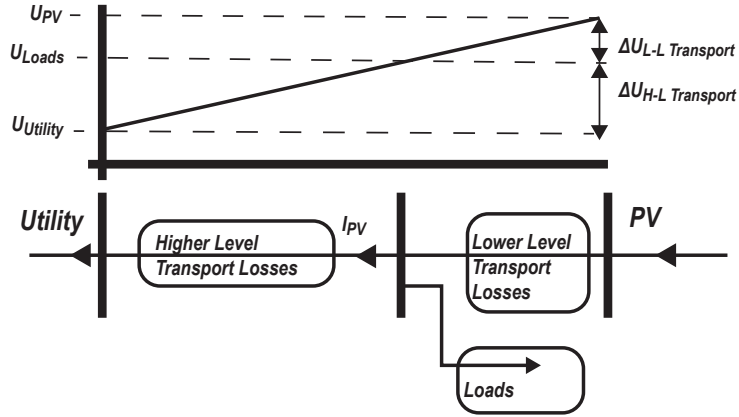


Figure 3.2: PV injection in lower levels of the network leads to a voltage raise also at higher levels of the network.

However, if the load exactly matches the PV generation, there will be no voltage raise at the load. Moreover, it will reduce the slow voltage variations at the load, because no power support from the utility is needed [16]. PV systems usually operate at unity power factor [17], meaning that it only covers the active power load in the network. Therefore, the reactive power may still cause voltage variations.

3.1.3 Voltage Unbalance

Both single phase and three-phase PV systems can lead to current unbalance between the three phases. In the presence of an unbalanced load, three-phase

PVS can aggravate the unbalance in the network. This may lead to the PV system satisfying the load in one phase, but not the other. In the worst case, some phases may inject power in the external grid, while the other draws power.

3.2 EV Charger Systems

3.2.1 Definition

An Electric Vehicle (EV) is a battery powered car that requires an external power source to charge its battery. To provide this demand, EV Charging Systems, with available charging sockets, are installed.

3.2.2 Voltage Level and Unbalances

Depending on the connected EV(s) and EV charging stations, and the impedance of the network, there can be substantial network losses. In the same way as described in section 2.1.2 and section 2.2.2, these losses may result in voltage drops that risk undervoltage and unbalance at the system's feeder.

Part II

Ground Truth Data

Chapter 4

PV System Data Analysis

4.1 Background

The voltage at a certain node is the combination of the utility voltage and the in-between voltage drop. To analyze the effect of the PV system on the voltage drop, the current must be inspected. If the behaviour of the current is aligned with the behaviour of the node's voltage, there is a significant influence.

Current injection of PV systems can lead to voltage fluctuations in the feeder. Additionally, even with three-phase PV systems, voltage unbalances may be the result due to unbalanced currents. Although unbalanced loads alone may lead to voltage unbalances, the presence of a three-phase PV system may aggravate it.

In the Netherlands, the company HyTEPS has installed a monitoring device that monitors the power quality of a single household in a residential neighbourhood. The house has a 9 kWp PVS installed on its roof with a built-in measurement device.

In this analysis, raw data from the household and PVS was used to characterize the PVS effects on an electric network. The main points of focus were the slow voltage variation, and voltage unbalance. To do this, the three-phase line current, active and reactive power, and voltage were observed. The analysis was performed by plotting the data using Python.

4.2 Goal

The goal of the analysis is to characterize the PVS behaviour that lead to voltage unbalance and effects on the slow voltage variations.

Figure 4.1: Configuration of the household in the neighbourhood.

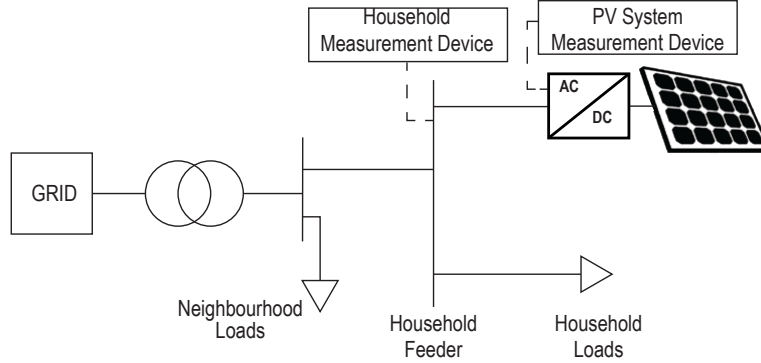


Figure 4.2

Table 4.1: PV Module Characteristics [18]

Brand	WINAICO
Total Capacity	~9kWp
Peak Power per Module	295 Wp
Amount Modules	30
Cell Surface	156.75*156.75 mm ²
Amount cells per Module	60
Module Efficiency	17.7%
Temperature Coefficient	-0.48%/K

4.3 Configuration

The configuration of the household system is shown in Figure 4.2. The house was located in a residential neighbourhood. Within this neighbourhood, other PV systems had been installed as well. In the monitored house, three-phase power was available, and a 9 kWp three-phase PV system was installed on the household's main feeder.

The household monitoring device was a SATEC EM133 Smart Energy Meter. It measured the voltage on the switchboard, and the current on the incoming feeder. The features of the PV modules are displayed in Table 4.1. The wires of the PV system were connected to the switchboard according to Table 4.2. The PV system had a monitoring device that measured the voltage and current on the AC and DC side of the converter.

4.3.1 Time Line

Two weeks of monitoring data was extracted from the months July and December 2018, which represented the best and worst sunlight conditions,

Table 4.2: Wiring of the PV System and the Household's main feeder.

Household	PVS
Phase L1	Phase L3
Phase L2	Phase L1
Phase L3	Phase L2

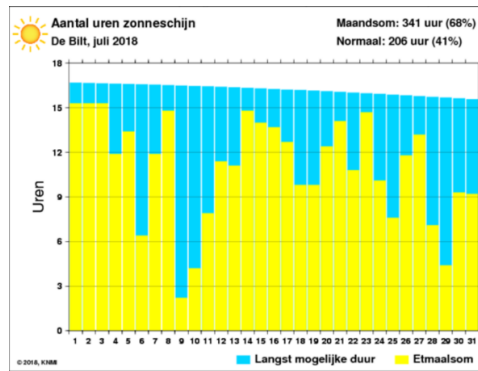


Figure 4.3: Sunlight recorded in July 2018, De Bilt, The Netherlands [19].

in that year. The amount of sunlight for both months are plotted in Figure 4.3 and Figure 4.4, respectively. Table 4.3 and Table 4.4 show the start and end times of the extracted monitoring data for the household and PV system measuring device, respectively.

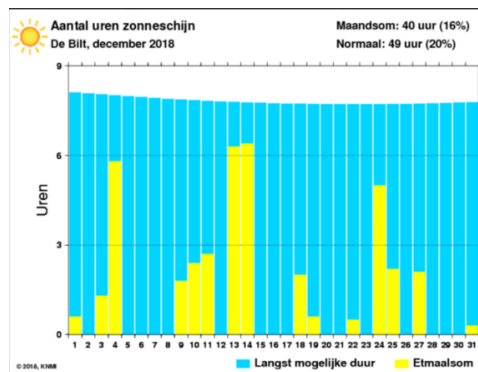


Figure 4.4: Sunlight recorded in December 2018, De Bilt, The Netherlands [20].


Table 4.4: Start and End times of the extracted PVS monitoring data.

PVS Monitoring	Start		End	
	Date (d/m/y)	Time (h:min)	Date (d/m/y)	Time (h:min)
July	15/7/2018	00:02	21/7/2018	23:54
December	16/12/2018	00:01	22/12/2018	23:56

Table 4.5: Values extracted from the Household and PVS monitoring data. X stands for extracted.

Name	Household Monitoring Device	PVS Monitoring Device
Date and Time	x	x
Three-Phase RMS Current	x	x
Three-Phase L-N Voltage	x	x
Three-Phase Active Power		x

Table 4.3: Start and End times of the extracted household monitoring data



Household Monitoring	Start		End	
	Date (d/m/y)	Time (h:min:s)	Date (d/m/y)	Time (h:min:s)
July	15/7/2018	00:16:06	21/7/2018	23:45:41
december	16/12/2018	00:33:26	22/12/2018	22:50:38

4.3.2 Data Extraction

Table 4.5 shows which values had been extracted from the monitoring data. The household monitoring device sent its measurements to a server where SATEC eXpertpower had been installed. The raw datasheet for the household monitoring device was acquired via this software. According to the data, the household monitoring device had sent values every 10 to 15 minutes. Sometimes, there were gaps of roughly 30 minutes in-between the recordings.

Raw data had been extracted from the PV system monitoring device directly. According to this data, the measurement device recorded the data every 5 to 6 minutes. These recordings also had a few gaps up to 14 minutes in-between the recordings.

This means that the data for both measurements were non-uniform. Furthermore, because of the different time recordings, the data from both devices cannot be exactly compared.

4.3.3 Processing

The extracted data was transformed into 12 and 30 minute averages to overcome the data's non-uniformity. Additionally, the neutral current caused by unbalanced currents was calculated, and the voltage unbalance was approximated, to evaluate its impact.

The reason for using the neutral current instead of the current unbalance is because current unbalance in percentages does not indicate the current difference in magnitude. For example, phase currents of 200A, 100A, and 50A have the same current unbalance as a set of phase currents of 2A, 1A, and 0.5A. However, the first set has a bigger influence on the voltage unbalance due to the higher magnitude of the current difference. In this example, the unbalance induced neutral current would be 132.29A and 1.32A, respectively.

12 minute Average

For the PV system data, a 12 minute average had been created according to Equation 4.1. Since the most common time gap between the recordings had been 6 minutes, most 12 minute average values were based on two measurements.

For every 12 minutes, starting at 0 : 00 :

$$\text{average data} = \frac{\text{Sum of Data}}{\text{Amount of Recordings}} \quad (4.1)$$

30 minute Average

For the household data, a 30 minute average had been created according to Equation 4.2. The amount of values, of which these averages were based upon, ranged from 1 to 3.

For every 30 minutes, starting at 0 : 00 :

$$\text{average data} = \frac{\text{Sum of Data}}{\text{Amount of Recordings}} \quad (4.2)$$

Neutral Current

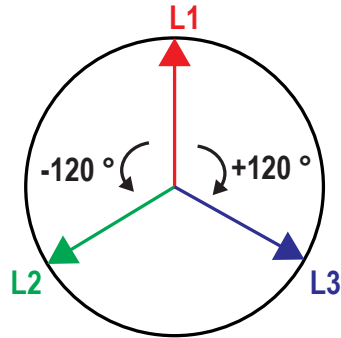


Figure 4.5: Phasor drawing of three-phase currents, in clockwise rotation, with a phase difference of 120°.

The neutral current induced by unbalance is the sum of the current phasors. However, only the RMS magnitudes of the phase currents are available in the measurements. This means that the phasor angles are not available.

Therefore, it is assumed that the phase difference between the phases is 120°, as shown in Figure 4.5. Then, the measured RMS current magnitudes and their respective phasor angles are used to calculate the neutral current according to Equation 4.3.

$$\bar{I}_0 = \bar{I}_{L1} + \bar{I}_{L2} + \bar{I}_{L3} \quad (4.3)$$

Voltage Unbalance

Similarly to the current, there are only RMS Magnitudes and no phasor angles available for the voltage measurements. Therefore, it is assumed that the phase difference between the phase voltages is 120°.

4.4 Results

4.4.1 Apparent Power

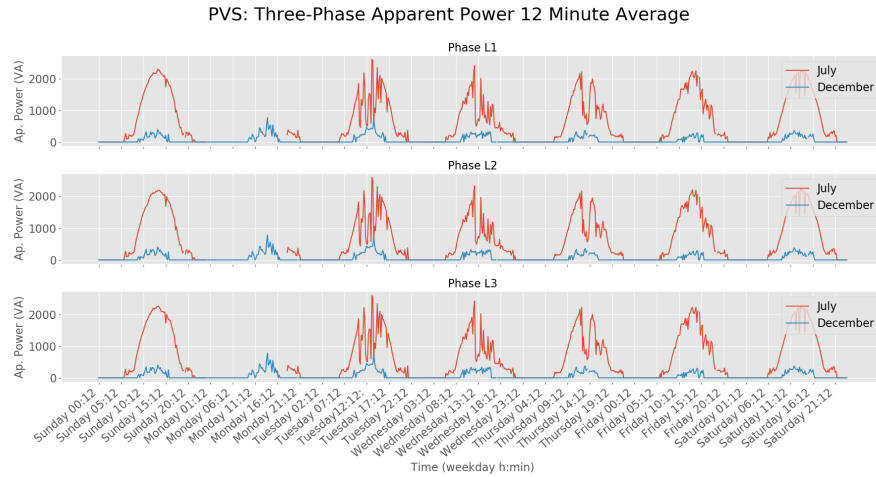


Figure 4.6: PVS: Three-Phase Power 12 minute Average

Figure 4.6 shows the recorded apparent power at the PV system.

4.4.2 Current Level

PV System

Figure 4.7 shows the PV system's three-phase 12 minute average current during a week in July and December. There was less current production in December than in July. The peak production in December was roughly 20% of the peak production in July. Additionally, the timespan where current was produced was shorter in December than in July. Current production in December occurred between 12:00 and 16:30, and between 5:00 and 23:00 in July.

The overall behaviour in July resembled a bell curve. This is expected, since the position of the sun, in relation to the PV modules, influences the solar irradiance on the modules. This curve was disrupted due to shading, which is represented by the current variations in the July curve.

In Figure 4.7, the July and December curves do not align. The December curve is slightly shifted to the left, in comparison to the July Curve. This is due to daylight saving time. In July, the clock is set an hour in advance, from UTC +1 to UTC +2, and leads to the PV curve shifting to the right.

Finally, the July curve had corners at the beginning and end of each day. To understand this phenomena, the apparent power had been calculated by multiplying the measured phase voltages and currents. This lead to Figure

4.8, where the measured active power was compared to the apparent power from Tuesday and Wednesday. This Figure shows that these injected powers, between 6:00 and 8:00, and between 18:30 and 21:00, exist of a significant amount of reactive power. At these particular time instances, there had not been enough electricity production, which lead to a non-optimal operation of the inverters. Additionally, Figure 4.9 shows that, in the December curve, the inverter was mostly in non-optimal operation.

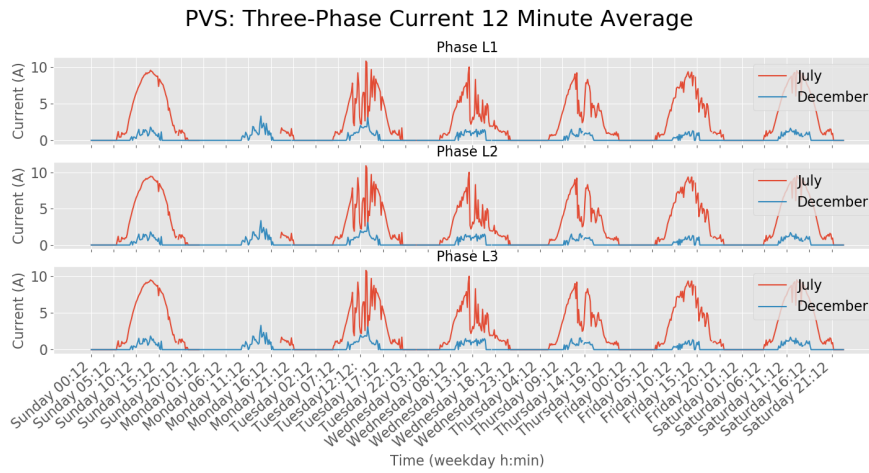


Figure 4.7: PVS: Three-Phase Current 12 minute Average

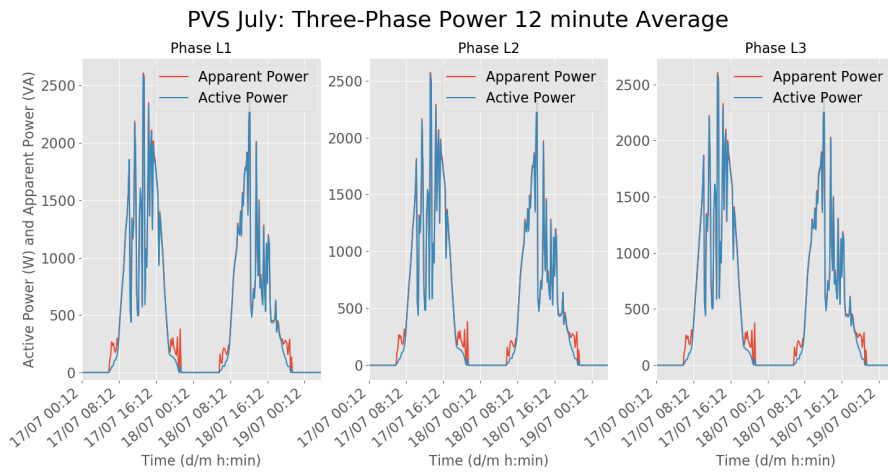


Figure 4.8: PVS July: Three-Phase Apparent Power and Active Power 12 minute Average

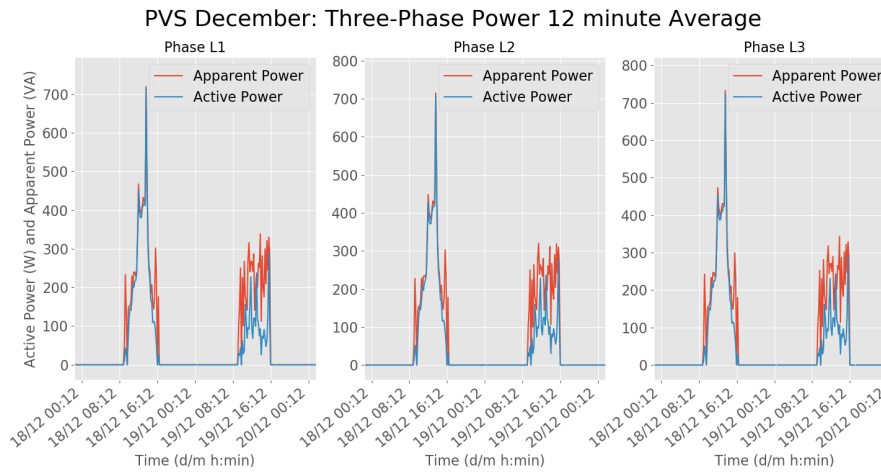


Figure 4.9: PVS December: Three-Phase Apparent Power and Active Power 12 minute Average

Household

Figure 4.10 shows the three phase current measured at the household feeder. In July, the PV curves are recognizable. This suggests that the household feeder was injecting current into the grid at this time. In December, this phenomena was less apparent, suggesting that the household was drawing current from the grid.

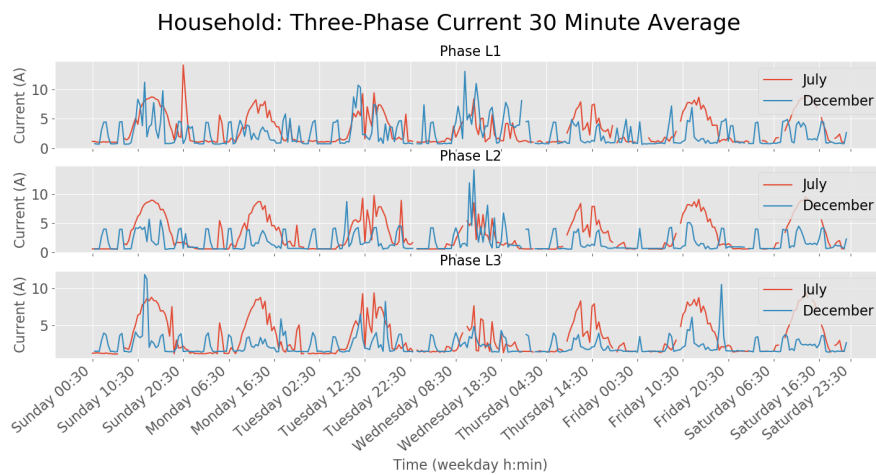


Figure 4.10: PVS December: Three-Phase Apparent Power and Active Power 12 minute Average

4.4.3 Current Unbalance

PV System

Figure 4.11 shows the 12 minute average phase current difference of the PV system for July and December. Differences L1-L2, L2-L3, and L3-L1, represent the absolute phase current magnitude difference between phases L1 and L2, L2 and L3, and L3 and L1, respectively. The current difference was up to 0.15 A. The unbalance results in the neutral current presented in Figure 4.12. The highest recorded neutral current was 0.14 A. The neutral current is 1.3% of the maximum current of 10.8 A measured in July.

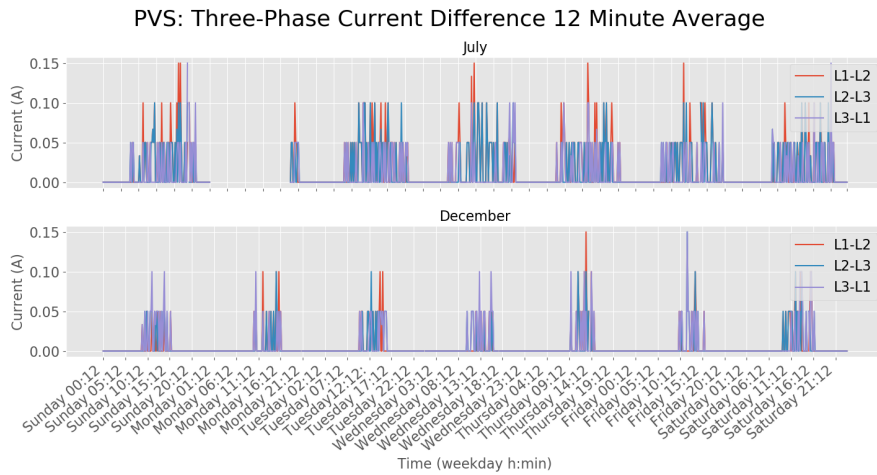


Figure 4.11: PVS: Three-phase Power Factor and Current

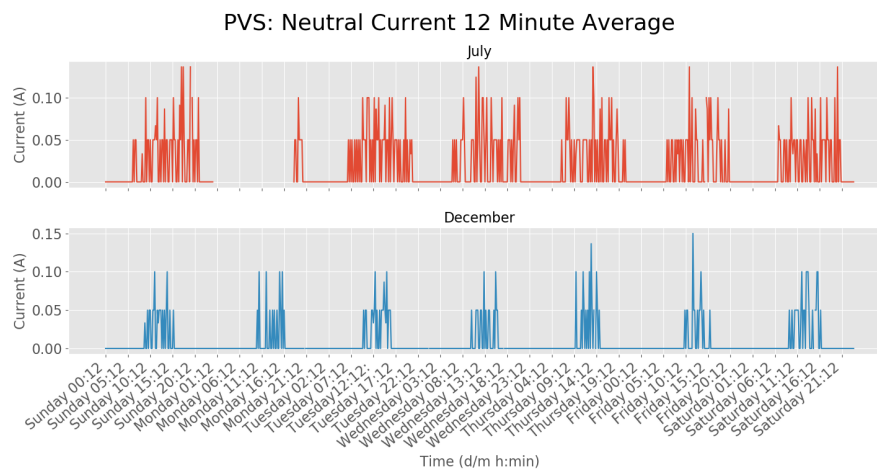


Figure 4.12: PVS: Neutral Current 12 Minute Average

Household

Figure 4.13 shows the difference in phase current, measured at the Household's feeder. The phase current difference was higher than the phase current difference at the PV system's feeder. This implies that this current unbalance was caused by the combined unbalanced loads and balanced generation at the household's main feeder.

In December, there were overall more phase current differences, than in July. As the current differences exceeded the current differences at the PV system, it seemed that the different neutral currents between July and December was mainly due to changes in loading.

The neutral current caused by unbalances is presented in Figure 4.14. The household showed neutral currents up to 12 A in July and December. This is consistent with calculated current differences.

Finally, Figure 4.15 shows the neutral current while the PV system was injecting current. This figure shows that the largest neutral currents were present during PV generation.

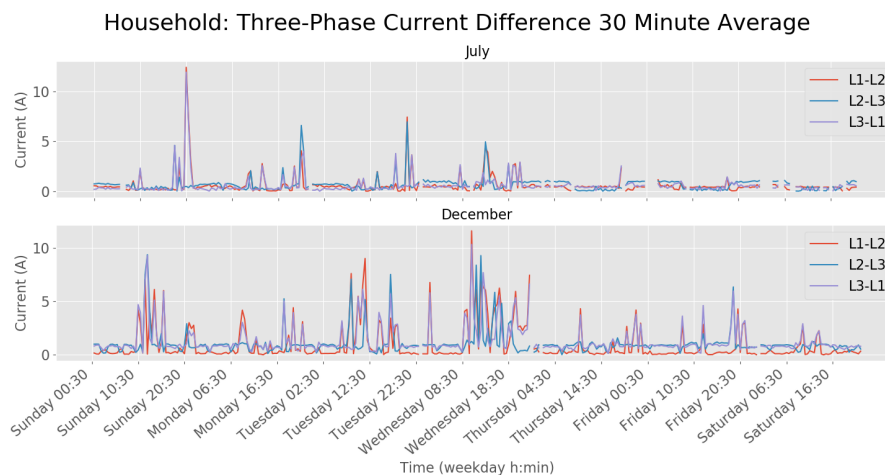


Figure 4.13: Household: Three-phase Current Difference 30 Minute Average

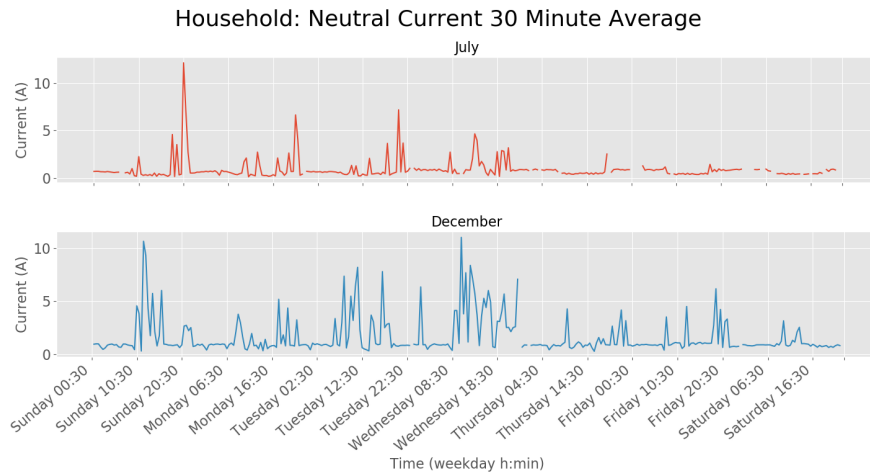


Figure 4.14: Household: Neutral Current 30 Minute Average

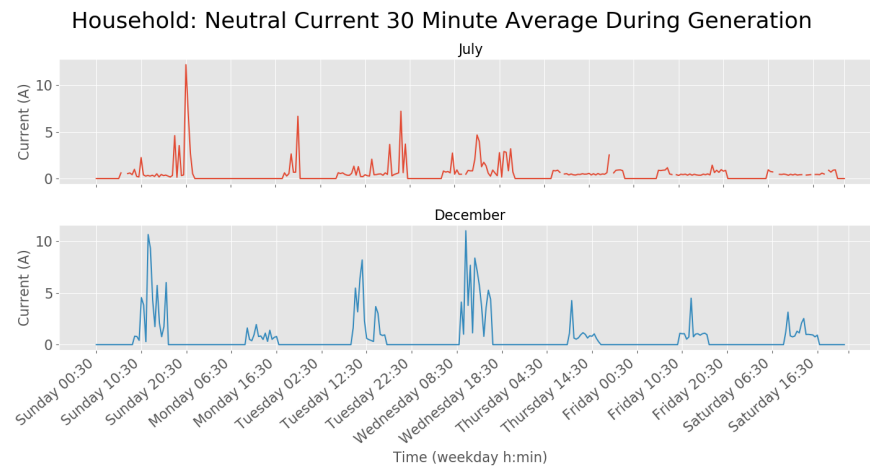


Figure 4.15: Household: Neutral Current 30 Minute Average During Generation

4.4.4 Voltage Level

PV System

Figure 4.16 and Figure 4.17 show the voltage vs current graphs for the PV system in July and December, respectively. In both figures, there is a clear rise in voltage, as current injection increases. However, in December, less current was produced overall, which lead to a small increase in voltage. Additionally, the PV systems installed in the rest of the neighbourhood influence the voltage as well.

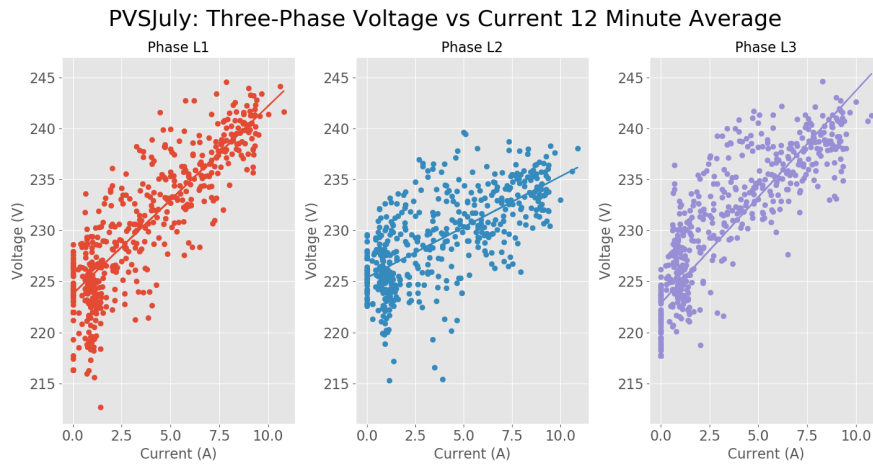


Figure 4.16: PVS July: Three-Phase Voltage vs Current 12 Minute Average. The dots represent the measurements, whereas the line represents the resulting regression plot.

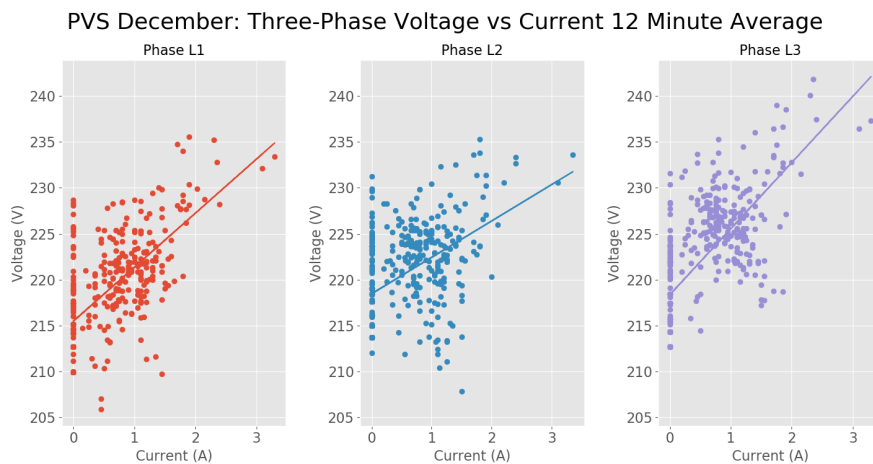


Figure 4.17: PVS December: Three-Phase Voltage vs Current 12 Minute Average. The dots represent the measurements, whereas the line represents the resulting regression plot.

Household

Figure 4.18 and Figure 4.19 show the voltage vs current graphs for the Household’s main feeder in July and December, respectively. By comparing Figures 4.18 and 4.16, both PV system and Household show similar behaviours. Remember that the PV system is wired as shown in Table 4.2.

Figures 4.19 and 4.17 show different behaviours. Here, the voltage on the

PV system rises to inject current into the main feeder. However, the loading behind the household's feeder is larger than generation. This results in the downwards or straight regression line.

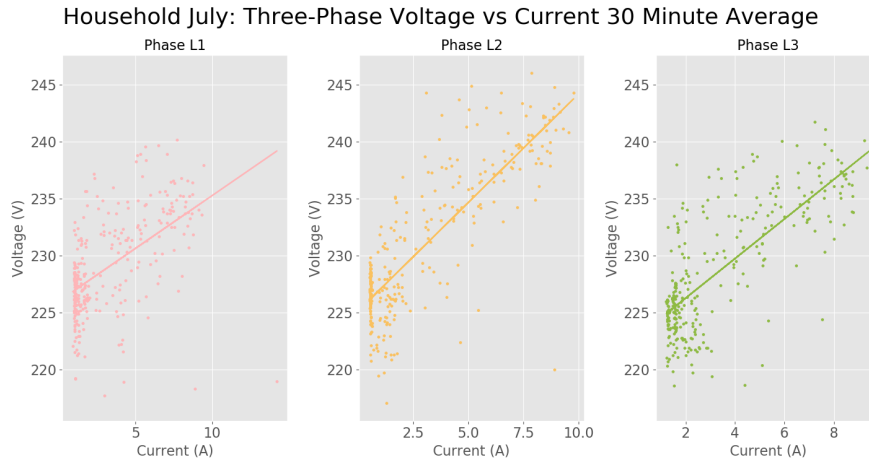


Figure 4.18: Household July: Three-Phase Voltage vs Current 12 Minute Average. The dots represent the measurements, whereas the line represents the resulting regression plot.

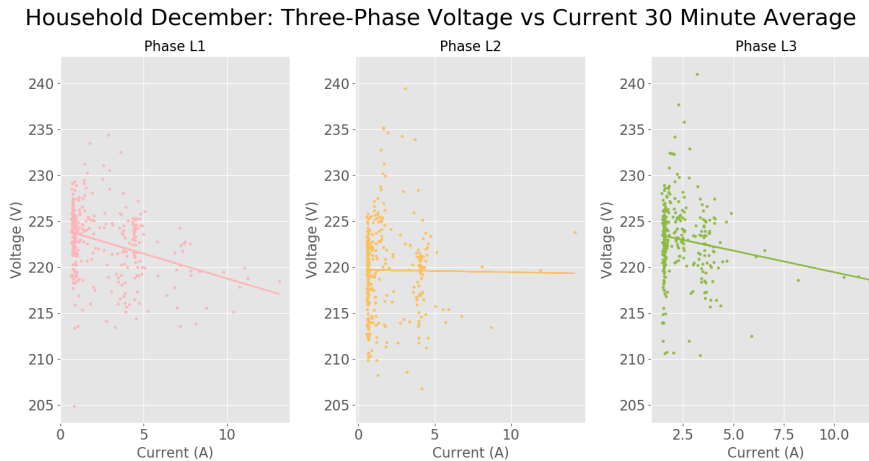


Figure 4.19: Household December: Three-Phase Voltage vs Current 12 Minute Average. The dots represent the measurements, whereas the line represents the resulting regression plot.

4.4.5 Voltage Unbalance

The voltage unbalance vs neutral current of both the PV system and Household data is plotted in 4.20. There was more voltage unbalances in Decem-

ber than in July. However, no clear relation was found between the voltage unbalance and the neutral current.

PVS and Household: Voltage Unbalance vs Neutral Current 30 Minute Average

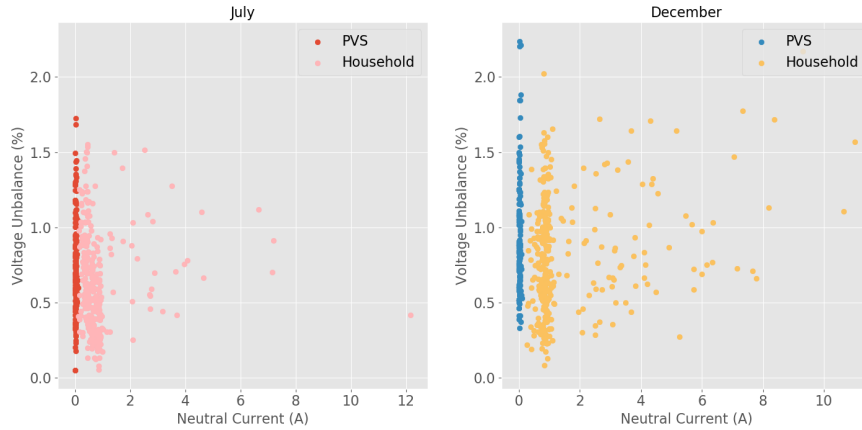


Figure 4.20: PVS and Household: Voltage unbalance vs Neutral Current

4.5 PV System Behaviour

In this analysis, raw data from the household and three-phase PV system was used to analyze the PV system effects on the electric network. The goal was to distinguish how PV affects the slow voltage variations and unbalances.

Figure 4.7 shows that the general behaviour of PV generation depends on the solar irradiance, the position of the sun, relative to the module, the amount of clouding during the day, and the characteristics of the PV system.

PV generation increases and decreases as the sun rises in the morning and sets in afternoon, respectively. There is more PV generation in Summer than in Winter. This is because the duration of daylight is longer, and there is generally less clouding, which is represented in Figures 4.3 and 4.4.

Additionally, PV generation depends on the characteristics of the PV system, namely the module characteristics, the angle placement of the module, and also the inverter. The behaviour of the inverter was noticeable in the measurements. Non-optimal operation of the inverter lead to the injection of reactive currents into the network as shown in 4.9. Nevertheless, the highest currents that may have a significant effect on the voltage were recorded at nominal operation of the inverter. Therefore, for determining the hosting capacity, it is correct to assume a unity powerfactor.

However, the connected loads are also important to determine the total effect on the household's voltage.

The PV generation raises the voltage level on the PV system by injecting current as seen in 4.16. However, a significant raise at the main feeder will only occur if the generation exceeds the load at the main feeder. This was

shown in Figure 4.18 and Figure 4.19. In July, the generation exceeded the load, which caused a voltage raise. In December, the load exceeded production, which lead to a voltage decrease.

Although a three-phase PV system could cause a voltage unbalance, in this analysis, there was too little connection found between PV generation and voltage unbalance. Current unbalances during PV generation were established as shown in Figure 4.15. As the highest neutral currents were measured during generation, it seemed that PV generation aggravated the current unbalance. However, it did not affect the voltage unbalance significantly.

Daylight savings time should be considered as well. Although these different times do not affect the position of the sun, relative to the module. Daylight savings time does affect human behaviour, and therefore the time at which loads are used.

Chapter 5

Electric Vehicle Chargers Data Analysis

5.1 Background

EV charger systems (EVCS) can affect the slow voltage variations and unbalances. The line current combined with the network impedance cause voltage drops and reduces the load voltage. Moreover, the difference in phase current will lead to voltage unbalances. Both phenomena can be found by measuring the three-phase voltage RMS magnitude and current.

The company HyTEPS had observed the power quality effects of commercial EVCS at an office site at an urban area in the Netherlands. In this research, the raw data from these measurements was used to analyse the EVCS effects on slow voltage variations and voltage unbalances. To do this, both the RMS of the line current and three-phase voltage were observed. The analysis was performed by processing and plotting the data using Python.

First, the goal of the analysis is explained, followed by the set-up of the analysis. Here, the original configuration of the previous measurement is defined. Then, the extraction and processing of the data for this analysis is explained. This is followed by the results of the analysis, and finally a conclusion

5.2 Goal

The goal of the analysis is to characterize the EVCS load behaviour that lead to influences on the voltage unbalance and slow voltage variations.

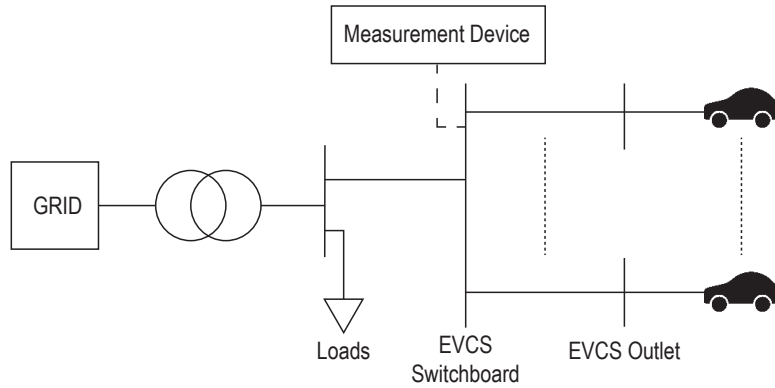


Figure 5.1: Configuration of the Measured network.

Table 5.1: Start and end times of the EVCS measurement.

First Measurement		Last Measurement	
Date (d/m/y)	Time (h:min:s)	Date (d/m/y)	Time (h:min:s)
21/08/2018	10:39:49	24/08/2018	10:22:29

5.3 Set-Up

5.3.1 Configuration

As shown in Figure 5.1, a total of 16 EVCS sockets had been installed on the EVCS main feeder. This was connected to the main distribution feeder, which was connected to a transformer and finally the grid.

The measurement device measured the voltage on the EVCS switchboard and the current on the incoming feeder of the EVCS switchboard. The measurement device was a portable device called the Fluke 435-II Power Quality Analyzer [21].

5.3.2 Timeline

Table 5.1 shows the start and end times of the measurement. The measurement was conducted during the course of three working days. At the start of the measurement 16 cars were connected.

5.3.3 Data Extraction

In the previous Part Theory, it had been explained that the voltage level is affected by the current combined with the transport impedance. Moreover, unbalanced currents lead to an unbalanced voltage. However, instead of using the current unbalance, the neutral current was used to indicate the

impact of current unbalance. This is because current unbalance in percentages does not indicate the phase difference magnitude.

Therefore, the following raw data had been extracted from the Fluke:

1. 10 seconds Average Three-phase RMS Current
2. 10 seconds Average Three-phase RMS L-N Voltage
3. 10 seconds Average Voltage Unbalance
4. 10 seconds Average Neutral Current
5. Date and Time

To evaluate the load based on its slow voltage variations influence and unbalances, the measurement data was transformed into 10 minute averages. This was achieved using Equation 5.1. Here, t represents the time steps of the raw data.

For $t = 1..2..3..4..$

$$10 \text{ min average data}(t) = \frac{\sum_{i=60t-59}^{60t} \text{data}(i)}{60} \quad (5.1)$$

The Fluke calculated the voltage unbalance according to the IEC suggested method [21].

Finally, all 10 minute averages were plotted and analyzed using Python.

5.4 Results

5.4.1 Apparent Power

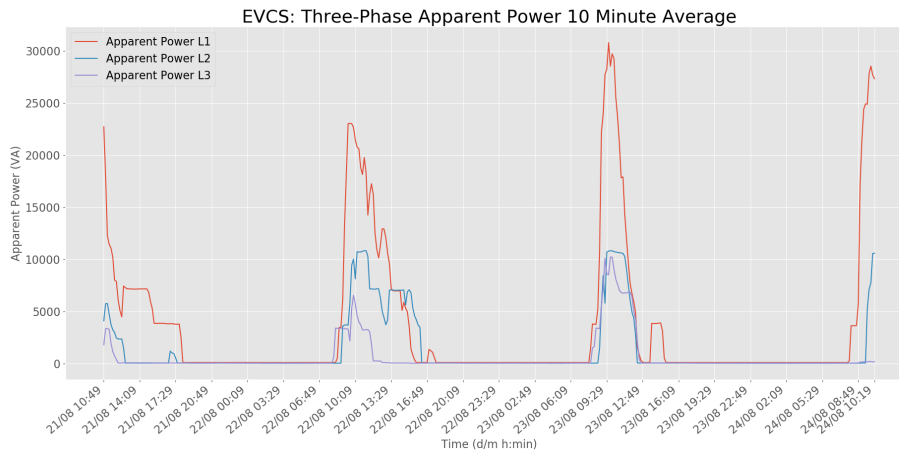


Figure 5.2: The Three Phase Apparent Power

Figure 5.2 shows the apparent power measured at the EV charging system.

5.4.2 Current Level

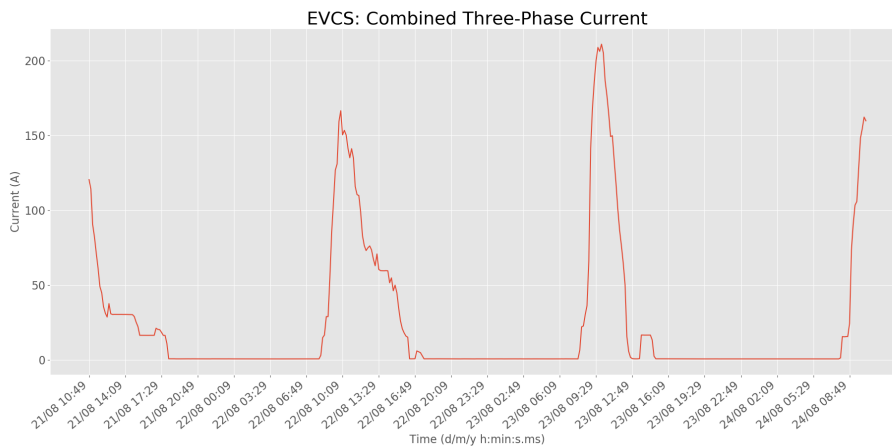


Figure 5.3: The total combined current

Figure 5.3 shows the combined three-phase current of the total recording period. It appears that most cars had been connected starting in the morning. No cars were connected after 19:00.

The highest loads were recorded at 10:49 on day 1, 9:29 on day 2, 9:39 on day 3, and 9:59 on day 4. However, day 1 and day 4 were not fully recorded.

On day 2, the current in phase L1 raised from 0 A to 167 A within 70 minutes, starting at 8:19. On day 3, the current raised from 0 A to 211 A within 110 min, starting at 7:49. The flow of current ended at 17:39, and 14:59 on day 2 and day 3, respectively.

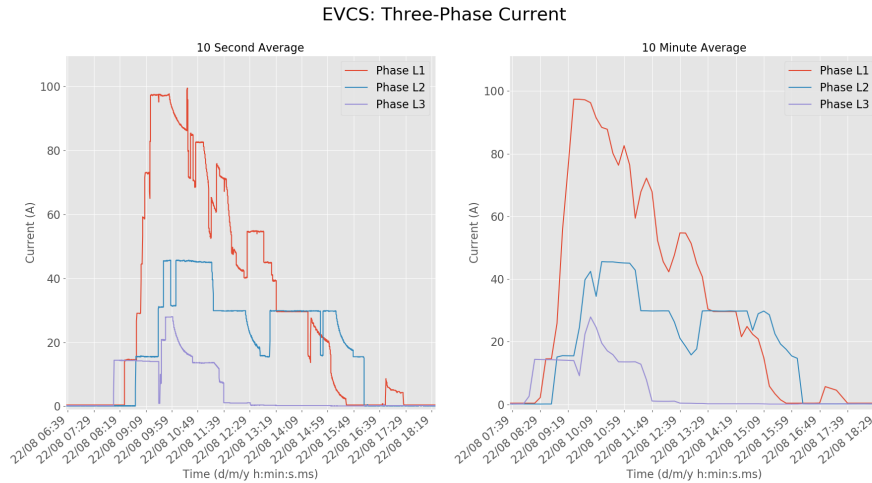


Figure 5.4

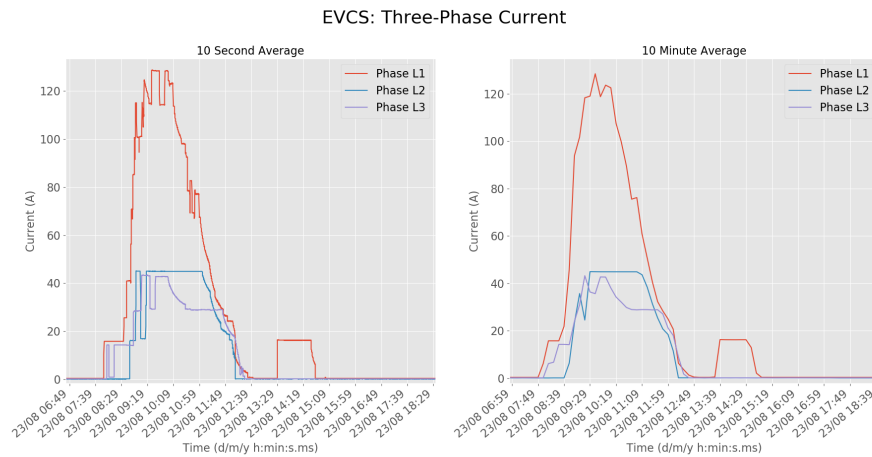


Figure 5.5

Figure 5.4 and Figure 5.5 show the 10 second and 10 minute comparison of individual phase currents for for day 2 and 3, respectively. It shows that the 10 minute average current increase in the morning was the cause of a

continuous summation of similar size step responses, of roughly 16 A. The declining of the current were both caused by step and smooth decrease.

On day 3, in Figure 5.5, at around 13:30, the pattern of current showed a block with an indented corner. Since there was no deviating behaviour, and as the maximum current was around 16 A, it is assumed that this pattern represented a single car. The single car showed a step increase, followed by a smooth decrease and step decrease, which seems to represent the connection, later battery stages, and disconnection, respectively.

This supports the fact that the summation of step responses was the result of multiple cars being connected. Subsequently, the drop in current was either due to disconnection or later battery stages. However, it isn't clear whether the disconnection was performed by the battery control or the user.

Finally, since day 3 had a higher maximum current than day 2, it appears that more cars were connected in the morning of day 3 than of day 2. However, day 2 had more cars connecting later during the day. This is shown by the bigger amount of deviations after the maximum current.

5.4.3 Current Unbalance

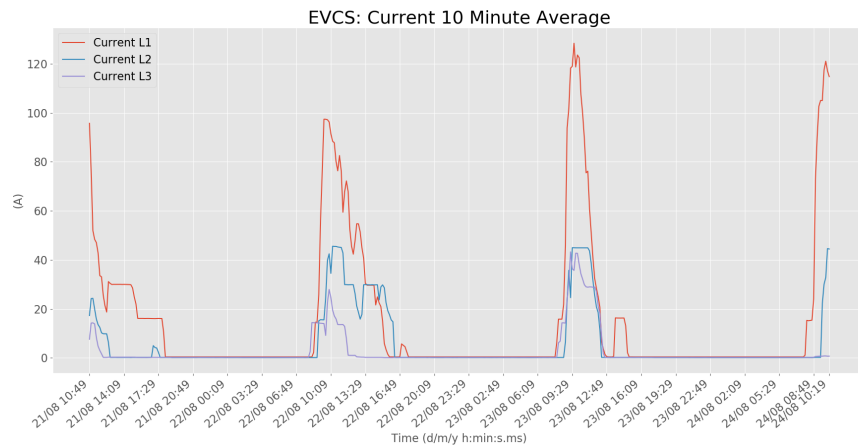


Figure 5.6

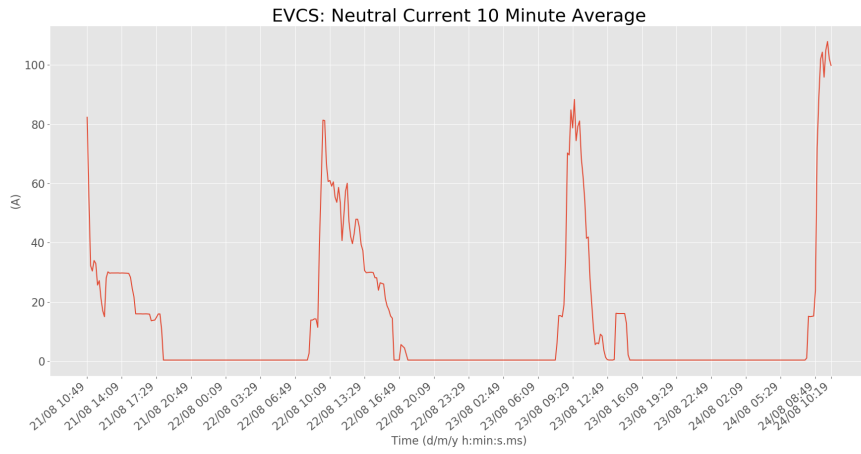


Figure 5.7

Figures 5.6 and 5.7 show the measured phase currents and measured neutral current. Figure 5.6 shows that most current flow was present in phase L1, whereas phase L3 had the least current flow. The current unbalance lead to a neutral current.

5.4.4 Voltage Level

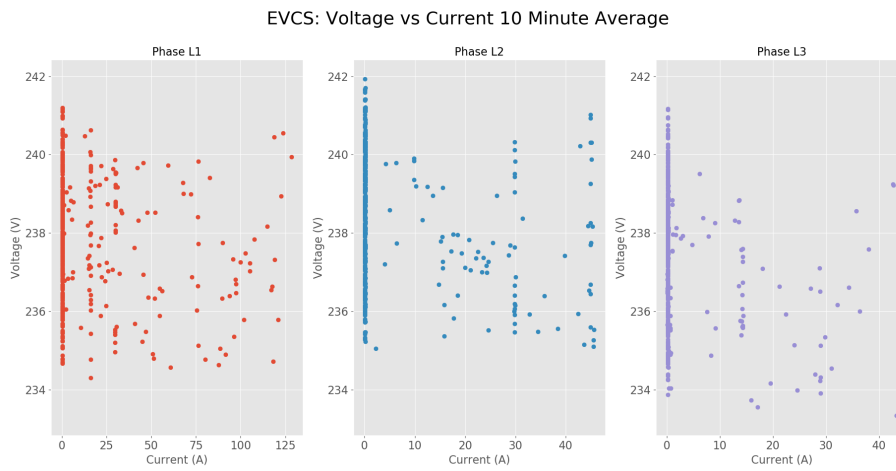


Figure 5.8

Figure 5.8 shows the 10 minute average voltage versus the 10 minute average current. The average voltage was 237.8 V, 238.4 V, 237.4 V, for phase L1, L2, and L3, respectively. There is no clear relation between the voltage and the current in each phase.

5.4.5 Voltage Unbalance

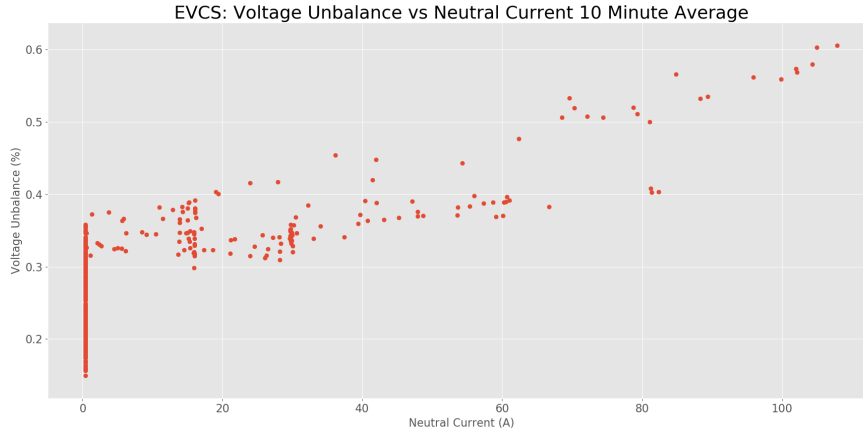


Figure 5.9

Figure 5.9 shows the 10 minute averages of the voltage unbalance versus the neutral current. There seemed to had been a linear relationship between the neutral current and the voltage unbalance percentage. The voltage unbalance percentage, according to both methods, raised around 0.3 % between a neutral current of 20 and 120 A.

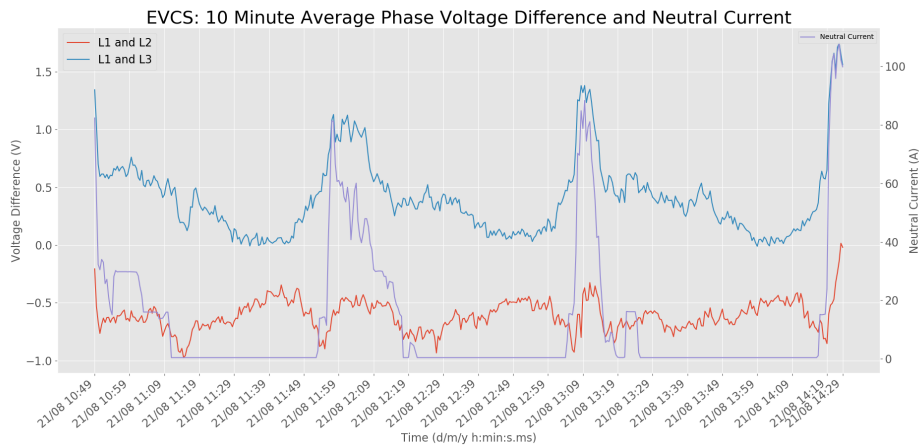


Figure 5.10: Voltage Phase Differences in voltage, according to Equation 5.2 and Equation 5.3, versus the neutral current.

$$\Delta U_{L1-L2}(t) = U_{L1}(t) - U_{L2}(t) \quad (5.2)$$

$$\Delta U_{L1-L3}(t) = U_{L1}(t) - U_{L3}(t) \quad (5.3)$$

Figure 5.10 shows the voltage difference between phase L1 and L2, and L1 and L3, and the neutral current. The phase voltage difference was calculated according to Equation 5.2 and Equation 5.3. Here, ΔU represents the phase difference in Volts, and U_{Lx} is the voltage in phase x . This Figure shows that the relationship, in Figure 5.9, was not in direct correlation with the current flowing through phase L1. If the current had influenced the phase voltage, by creating a bigger voltage drop in phase L1, the voltage in phase L1 should had gotten lower in comparison to phase L3. Instead, the voltage in phase L1 did the opposite. This means that the voltage was mostly the reflection of the source voltage.

5.5 EV Charging Behaviour

In this analysis, the raw data from a power quality measurement, performed by the company HyTEPS, was used to research the EVCS effects on the electric network. The observation was conducted at an office site in an urban area in The Netherlands. The goal of the analysis was to characterize the EVCS load behaviour that lead to influences on the voltage unbalance and slow voltage variations.

Results show that the power behaviour of EVCS depend on the the time at which cars are connected, the time that it takes to charge a car, the maximum phase power of the cars and the charger, the amount of cars connected, and finally the three-phase charging capability of the cars and chargers.

Figure 5.3 shows the car connecting behaviour related to the office workers. The same type of behaviour had been recorded in [22] and [23]. Generally known office times in the Netherlands are between 9:00 and 17:00. This was represented by the EVCS behaviour during the measurement, considering that the first and last people arrive and leave, respectively, up to an hour and a half outside office times.

Subsequently, a high charging peak is expected in the morning. This is followed by a period where more cars are disconnecting, than connecting. This could be due to the fact that drivers do not tend to move their car when their battery is full, decreasing available space [23]. It is therefore possible that, due to this reason, at the end of the working period, another driver decides to charge their car. Usually, this peak is small, as shown in 5.3 and in [22] and [23].

The time of connection also affects the daily duration of the charging. If connection is more spread out during the day, it is expected that the charging duration is longer. However, if the connection happens within a

short time frame, the total duration is shorter. This difference is shown in Figures 5.4 and 5.5.

The total amount of drawn power also depends on the type of cars, chargers, and amount of cars connected. Electric vehicles differ in charger capabilities. However, the charger must be able to support it as well [24]. During the measurements, considering Figures 5.4 and 5.5, it seemed that either the chargers, or every EV, was limited up to around 16 Amps per phase. Finally, the amount of charging cars determine the total amount of power.

The three-phase capabilities of the cars and chargers affect the current unbalance. Both cars and chargers can be characterized as to only support single phase charging. This leads to unbalanced currents as shown in 5.8.

However, the total effect on the voltage depend on both the utility voltage and voltage drop. Figures 5.9 and 5.10 show that the unbalance did not have a significant impact on the voltage drop and therefore it can be determined that the combined current and impedance did not have a significant influence.

Chapter 6

Network Data Analysis

6.1 Background

EV charger systems and PV systems introduce additional currents into the network. These currents may raise the voltage or cause unbalanced voltages in the installation. However, the magnitude of this effect is dependent on the total combined three-phase current and network impedance. Therefore, it is important to analyze the loads and impedances of the network without the inclusion of EV charger or PV systems.

In this analysis, two weeks of real monitoring data, provided by a client from the company HyTEPS, was analyzed. The data contains information about the powers, currents, and voltages measured at four different installations. Each of these installations represent a loaded LV network connected to the MV network. This data was used to evaluate the hosting capacity of either PV or EV charger systems later in this thesis.

6.2 Goal

The goal of the analysis is to characterize the network's impedance and load behaviour that risk the voltage level and voltage unbalance, when either a PV system or EV charger system is added.

6.3 Set-Up

6.3.1 Configuration

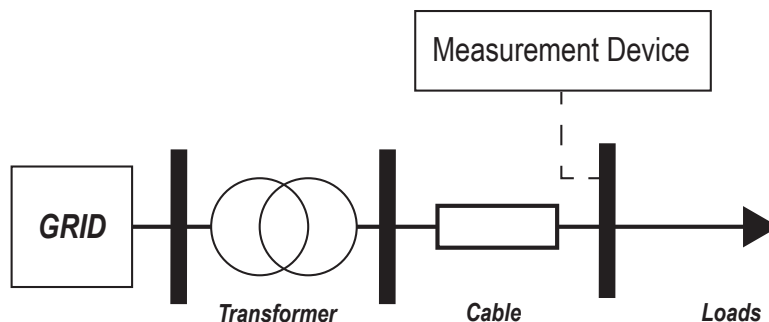


Figure 6.1: Configuration of the Measured network.

Figure 6.1 shows the network configuration and placement of the measurement device. From left to right, the analyzed network contains the grid, a MV/LV transformer, a cable in-between the transformer and the main distribution feeder, and loads at the main feeder. In each of the five cases, the monitoring device measured the distribution feeder directly behind the transformer that connected the LV network to the MV network.

6.3.2 Time Line

Table 6.1: Start and End times of the provided monitoring data.

Start		End	
Date (d/m/y)	Time (h:min:s)	Date (d/m/y)	Time (h:min:s)
02/12/2018	00:15:00	16/12/2018	00:00:00

Table 6.1 shows the start end times of the monitoring data provided by the client.

6.3.3 Data Extraction

Table 6.2: Transformer characteristics of each network

Network	Transformer Capacity	Transformer Ratio
N1	2500 kVA	10kV/420V
N2	1000 kVA	10kV/420V
N3	630 kVA	10kV/400V
N4	1000 kVA	1000kV/420V

Table 6.2 shows the information that was acquired about the transformers. Every 15 minutes, the monitoring devices saved the measurements. From these measurements, the following values were analyzed:

1. Three-Phase Active Power
2. Three-Phase Reactive Power
3. Three-Phase Current
4. Three-Phase Voltage
5. Date and Time

6.3.4 Processing

The impedance of the transformer is calculated using the transformer information, which is provided by the client. The maximum voltage drop case is assumed for the calculation of the cable impedance between the transformer and the main feeder. Finally, the neutral current and voltage unbalance was calculated in the same way as in section 4.3.3.

Transformer Impedance

The transformer's base impedance, Z_{base} , impedance magnitude, $|Z_T|$, resistance, R_T and reactance, X_T , in ohm in each phase is calculated according to Equations 6.1-6.4 [25]. Here, cap is the total capacity of the transformer in VA , U_{sec} is the secondary voltage from Table 6.2 in V , $U_{T\ L-N}$ is the secondary line to neutral voltage, p_k in W and u_k in $\%$ are the short circuit loss and voltage, respectively. The values pk , and uk depend on the transformer capacity and are based on the Dutch norm [26].

$$Z_{base} = \frac{U_{T\ L-N}^2}{cap \cdot \frac{1}{3}} = \frac{\left(U_{sec} \cdot \frac{1}{\sqrt{3}}\right)^2}{cap \cdot \frac{1}{3}} \quad (6.1)$$

$$|Z_T| = U_k \cdot Z_{base} \quad (6.2)$$

$$R_T = \frac{P_k}{cap} \cdot Z_{base} \quad (6.3)$$

$$X_T = \sqrt{|Z_T|^2 - R_T^2} \quad (6.4)$$

Cable Impedance

As shown in Equation 6.5, the maximum drop, ΔU_{max} over the cable is 3% of the nominal voltage, U_{nom} , which is 230V. This means that the maximum voltage drop is equal to 6.9 V. Then, the cable resistance per phase, R_C , is calculated using the nominal current of the transformer, $I_{T\ nom}$, according to Equations 6.6-6.7. Since the LV network's resistance is considerably larger than the reactance [25], the cable reactance is neglected.

$$\Delta U_{max} = 0.03 \cdot U_{nom} \quad (6.5)$$

$$I_{T\ nom} = \frac{cap \cdot \frac{1}{3}}{U_{T\ L-N}} \quad (6.6)$$

$$R_C = \frac{\Delta U_{max}}{I_{T\ nom}} \quad (6.7)$$

Neutral Current and voltage unbalance

For the neutral current and the voltage unbalance, it is assumed that the phase difference between the phase values is 120° . By using the measured RMS currents and voltages, the voltage unbalance and neutral current were calculated according to Equations 2.2 and 4.3, respectively.

6.4 Results and Behaviour

6.4.1 Impedances

Table 6.3: Transformer and Cable impedance of the network

Name	Transf. Nominal Current (A)	Transformer Impedance (ohm)	Cable Imp. (ohm)	Total Impedance (ohm)
N1	3437	6.21E-4 + 4.19E-3j	2.01E-3	2.63E-3 + 4.19E-3j
N2	1375	1.85E-3 + 1.04E-2j	5E-3	6.85E-3 + 1.04E-2j
N3	909.3	2.62E-3 + 9.81E-2j	7.59E-3	10.2E-3 + 9.81E-2j
N4	1375	1.85E-3 + 1.04E-2j	5.02E-3	6.87E-3 + 1.04E-2j

Table 6.3 shows the impedance of the transformers and cables of the analyzed networks.

6.4.2 Network N1

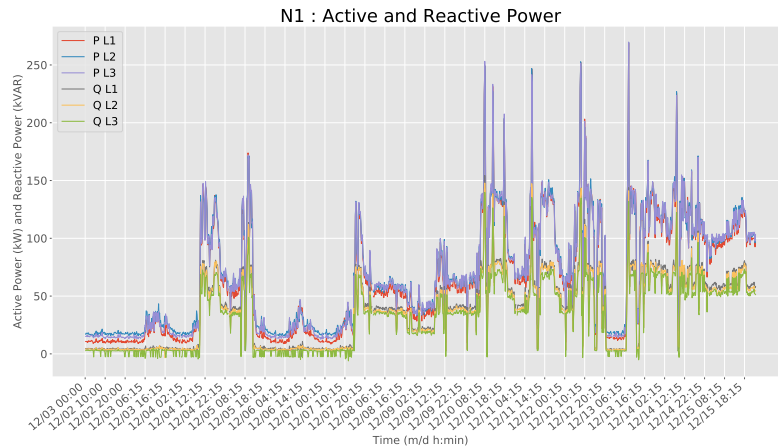


Figure 6.2: Active and Reactive Power of N1

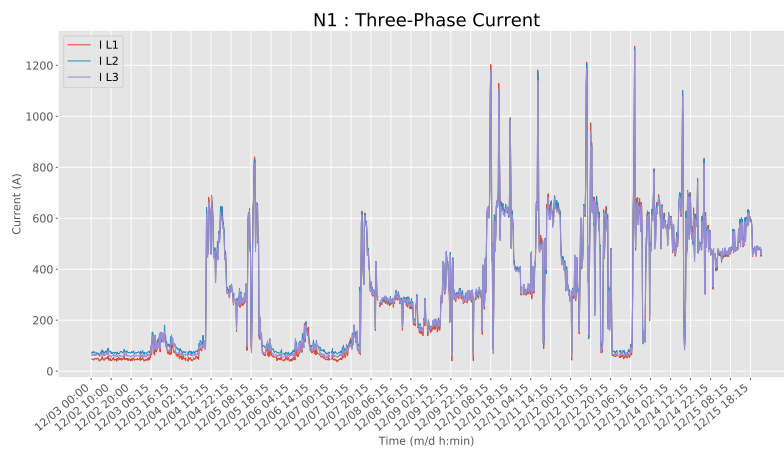


Figure 6.3: Three-Phase Current of N1

Figures 6.2 and 6.3 show the three-phase active and reactive power, and the current, respectively. Within this period, the maximum apparent power was 909.6 kVA, meaning that the transformer was loaded up to 36.3%. The minimum apparent power was 37.7 kVA, which is 1.51% of the available transformer loading.

Both active and reactive power was measured as positive. This meant that the reactive power was inductive. Subsequently, the power's related current contributed to the drop in voltage at the main feeder.

Furthermore, there does not seem to be a clear weekly or daily pattern in the power and the current. As a clarification, the dates 2/12, 8/12, 9/12 and 15/12 were weekend days.

The daily patterns do not match PV generation. Still, the largest power demands are recorded during daytime, which is beneficial for having PV generation.

The load behaviour isn't reliable considering EV charging. On 4/12, and 7/12, highest daily demand was recorded after 10:00. However, on 10/12 and 13/12 highest demand was recorded before 10:00.

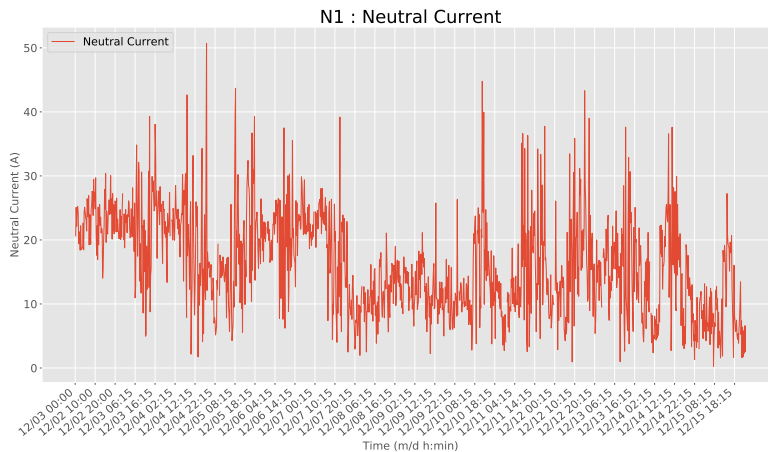


Figure 6.4: Neutral Current of N1

Figure 6.4 shows the neutral current at the main feeder. There isn't a clear pattern in the neutral current. The measured neutral current was up to 51 A. This is 1.5% of the nominal transformer current. Therefore, no significant effect on the voltage unbalance is expected.

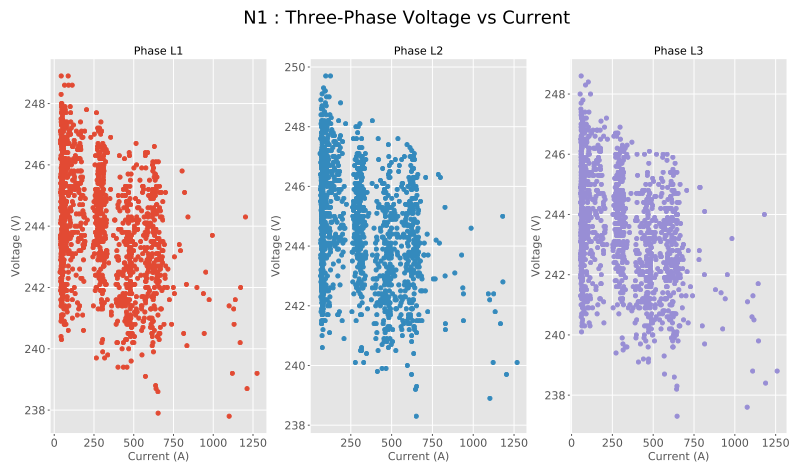


Figure 6.5: Voltage vs Current of N1

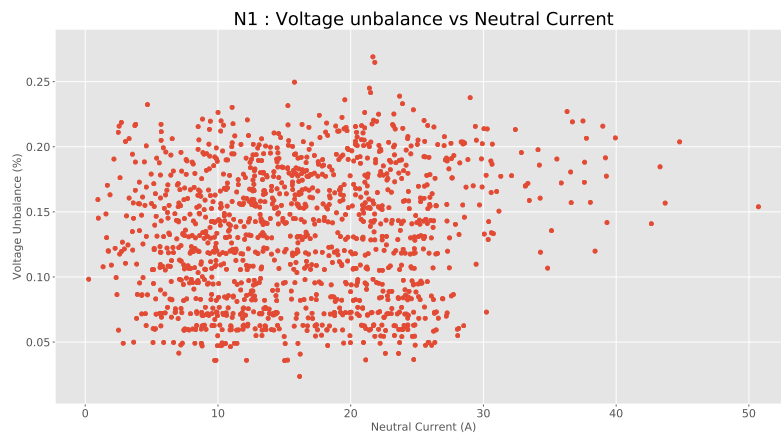


Figure 6.6: Voltage Unbalance vs Neutral Current N1

Figures 6.5 and 6.6 show the current and unbalanced current effect on the voltage level and voltage unbalance, respectively. As expected, the magnitude of the current difference is too low to show a significant effect on the voltage unbalance.

However, the magnitude of the current is sufficiently high. This is because a clear relation between the voltage and the current can be observed in Figure 6.5.

6.4.3 Network N2

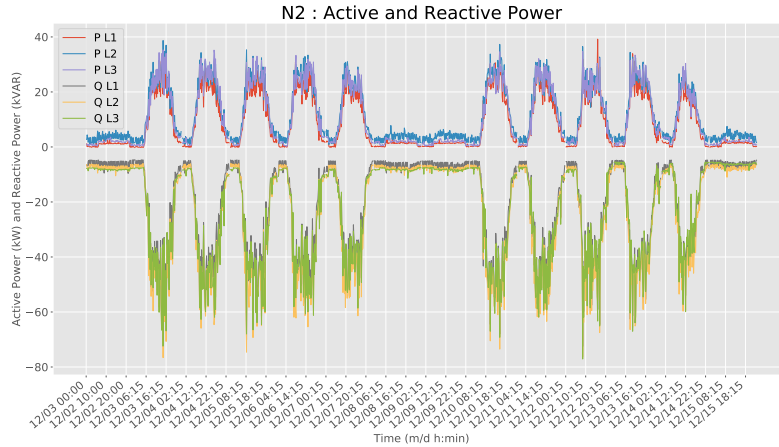


Figure 6.7: Active and Reactive Power of N2

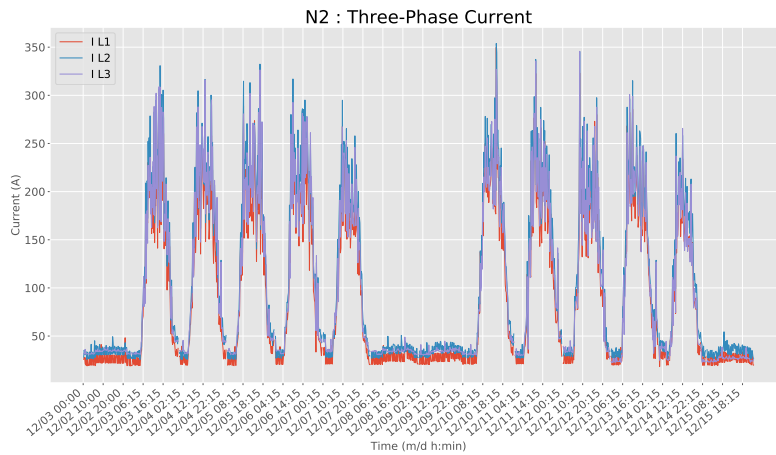


Figure 6.8: Three-Phase Current of N2

Figures 6.7 and 6.8 show the three-phase active and reactive power, and the current, respectively. The maximum and minimum apparent power was 248.3 kVA, and 16.8 kVA, respectively. This is 24.8% and 1.68% of the total transformer loading, respectively.

Throughout the acquired monitoring period, the reactive power was negative, meaning that the loads behind the feeder were capacitive. Therefore, reactive part of the current contributed to a voltage increase at the main feeder, whereas the active part contributed to a voltage decrease.

The load in network N2 has a clear pattern. Highest loads were recorded during weekdays, whereas the least load was recorded at night and in the weekends.

During weekdays, the load is comparable to the generation of PV. However, it will pose a problem during the weekends, because the load is considerably lower. Moreover, the reactive part of the load is higher than the active part, which cannot be covered by PV systems with a unity power factor.

For the hosting capacity of EV charging, an inverse pattern of the EV behaviour is desired. This means a load behaviour which is relatively low in the morning, and increases in the afternoon. However, in this case, the load increases, starting at 6:00, deviates between 20 and 40 Watts during the day, and decreases around 20:00.

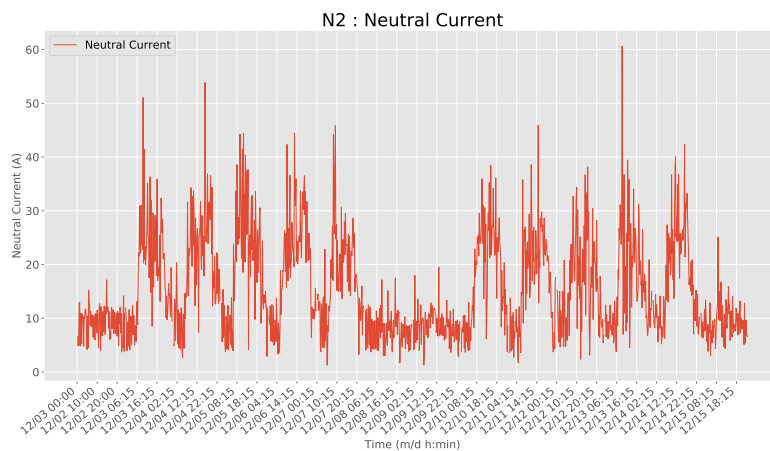


Figure 6.9: Neutral Current of N2

Figure 6.9 shows the neutral current of the network. The neutral current shows a similar pattern as the three-phase current. The highest neutral current is calculated at 61 A. This is 4.44% of the transformer's nominal current.

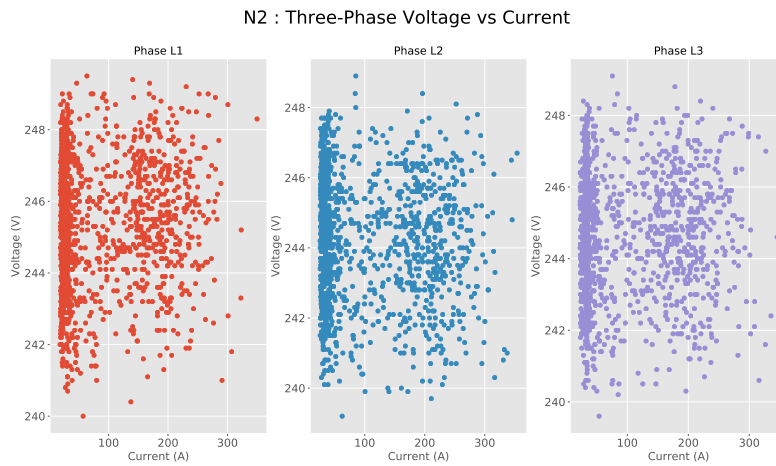


Figure 6.10: Voltage vs Current of N2

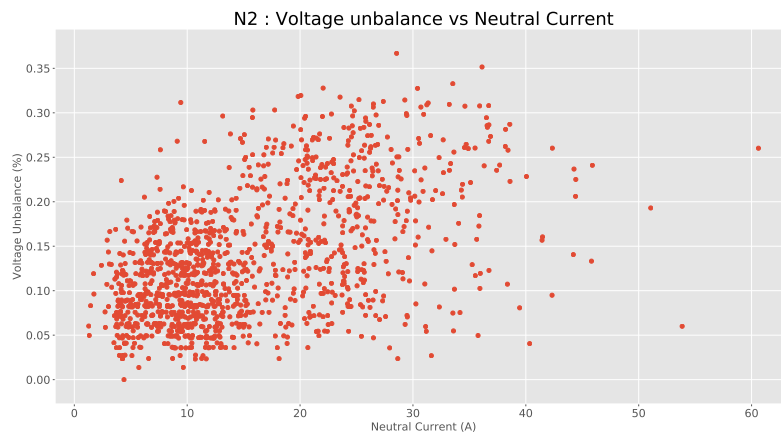


Figure 6.11: Voltage Unbalance vs Neutral Current N2

Figures 6.10 and 6.11 show the current and unbalanced current effect on the voltage level and voltage unbalance, respectively. There did not seem to be a relation between the three-phase voltage and current. However, this could have been caused by the higher capacitive current that compensated the voltage drop caused by the active current.

Finally, Figure 6.11 tends to show a small relation between the neutral current and the voltage unbalance. However, the relation is more noticeable than Figure 6.6, because the neutral current is relatively higher, considering the transformers' capacities.

6.4.4 Network N3

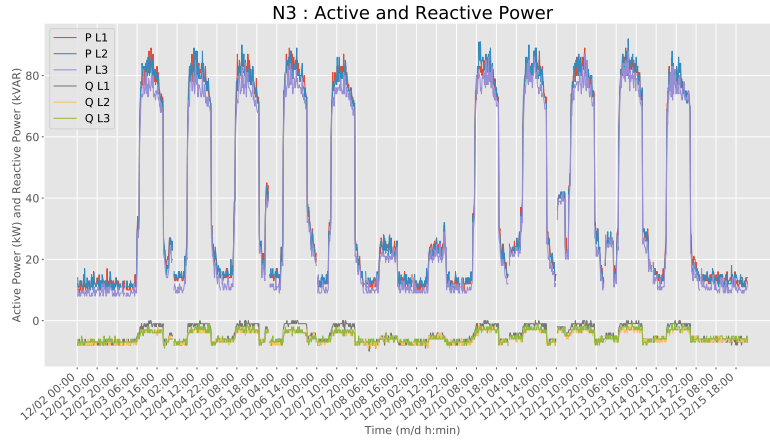


Figure 6.12: Active and Reactive Power of N3

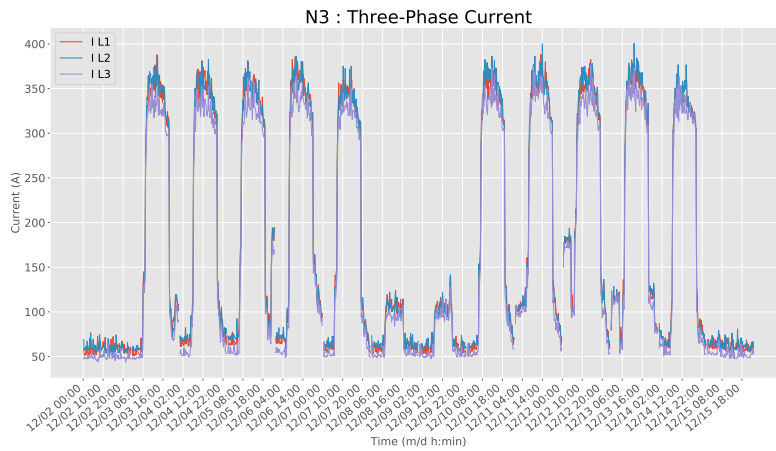


Figure 6.13: Three-Phase Current of N3

Figures 6.12 and 6.13 show the three-phase active and reactive power, and the current, respectively. Within this period, the maximum apparent power was 271 kVA, meaning that the transformer was loaded up to 43.0%. The minimum apparent power was 36 kVA, which is 5.71% of the available transformer loading.

The reactive power was capacitive in the weekends, and neared zero during the weekdays. This means that, in the weekends the reactive current contributed to a voltage rise at the main feeder.

The weekday pattern was very clear. However, both weekend patterns weren't the same. The load acted similarly to N2. Moreover, it had the same start and end times of the loads, with the exception of the weekend load. However, the change from no load to full load, in the morning, was more abrupt.

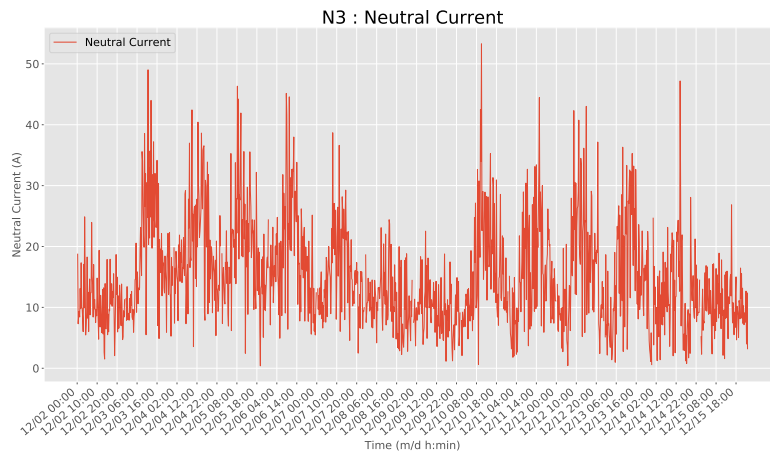


Figure 6.14: Neutral Current of N3

Figure 6.14 shows the neutral current of the network. The maximum neutral current is 53 A, which is 5.8% of the nominal current.

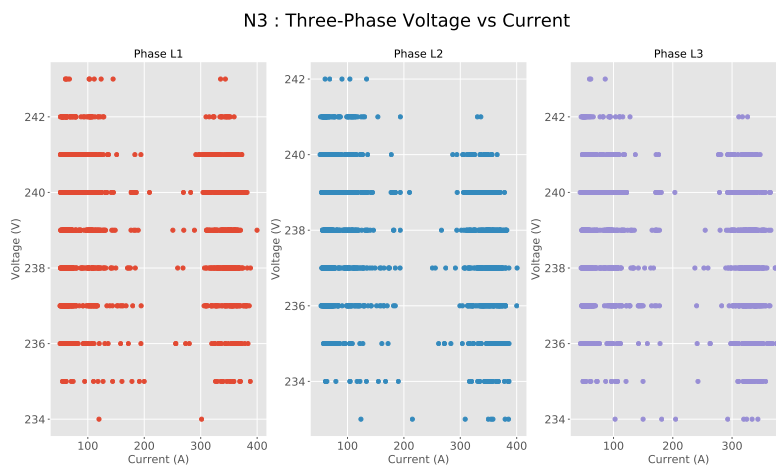


Figure 6.15: Voltage vs Current of N3

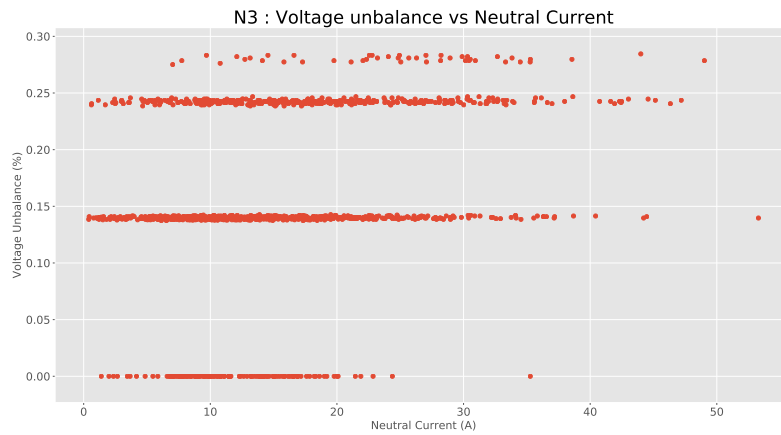


Figure 6.16: Voltage Unbalance vs Neutral Current N3

Figures 6.15 and 6.16 show the current and unbalanced current effect on the voltage level and voltage unbalance, respectively. These Figures show there is a difference in measurement accuracy between network N1 and N3.

There wasn't a clear relation between the phase current and the phase voltage. A relation was expected, considering that the transformer was loaded up to 43 %. However, it was possible that the network impedance was lower than expected. On the other hand, the accuracy of the voltage measurements, could have made it difficult to determine a pattern between the voltage and the current.

Similarly to network N1 and N2, the voltage unbalance is not significant. However, a relation between the neutral current and voltage unbalance could be established.

6.4.5 Network N4

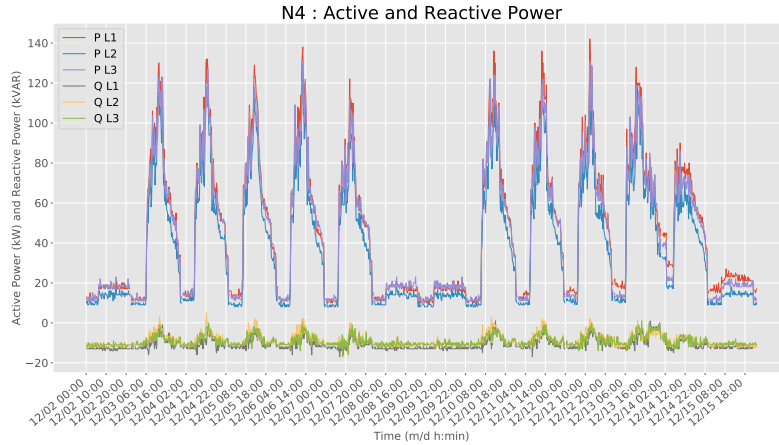


Figure 6.17: Active and Reactive Power of N4

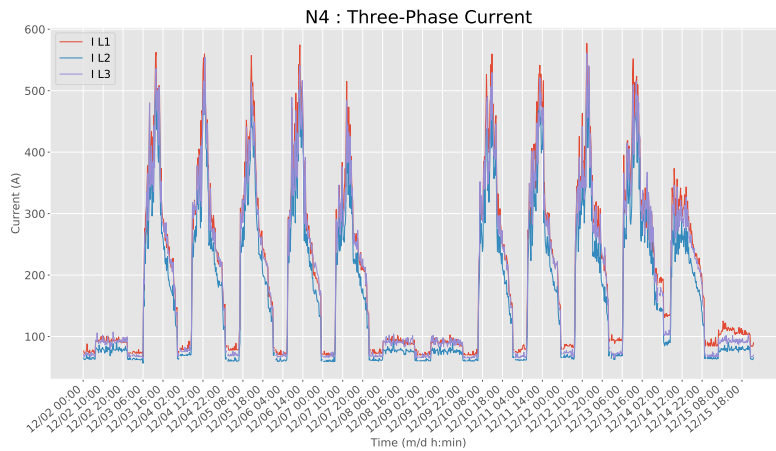


Figure 6.18: Three-Phase Current of N4

Figures 6.17 and 6.18 show the three-phase active and reactive power, and the current, respectively. Within this period, the maximum apparent power was 404 kVA, meaning that the transformer was loaded up to 40.4%. The minimum apparent power was 45 kVA, which is 4.5% of the available transformer loading.

Network N4 showed a clear pattern in daily loading during the weekdays and the weekend. In the weekends, the reactive power was capacitive, meaning that here, the current contributed to a voltage raise at the main

feeder.

During the weekdays most of the loading is expected in the morning and early afternoon. In the weekends, the loading is significantly lower. It is expected that the installation capacity of the PV system is limited by this.

For EV charger systems, the loading isn't ideal, as most of the main feeder loading is situated around the morning and early afternoon.

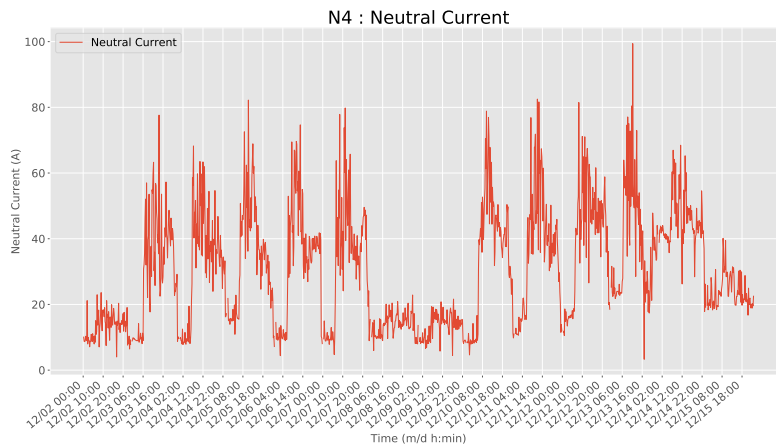


Figure 6.19: Neutral Current of N4

Figure 6.19 shows the neutral current of the network. The maximum neutral current is 99 A, which is 7.2% of the nominal current.

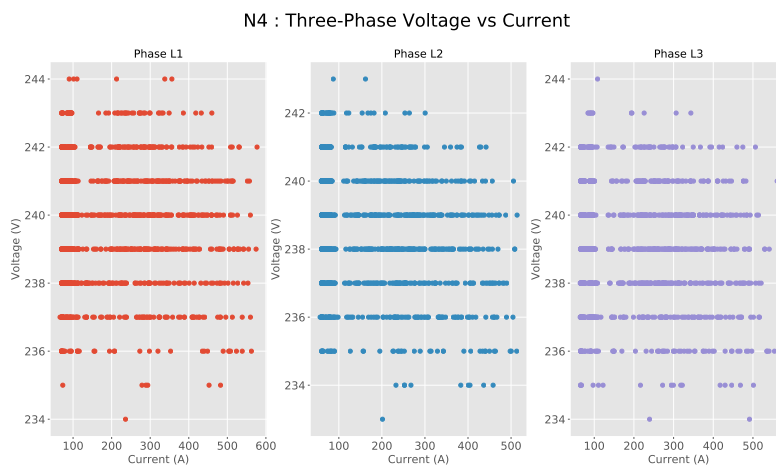


Figure 6.20: Voltage vs Current of N4

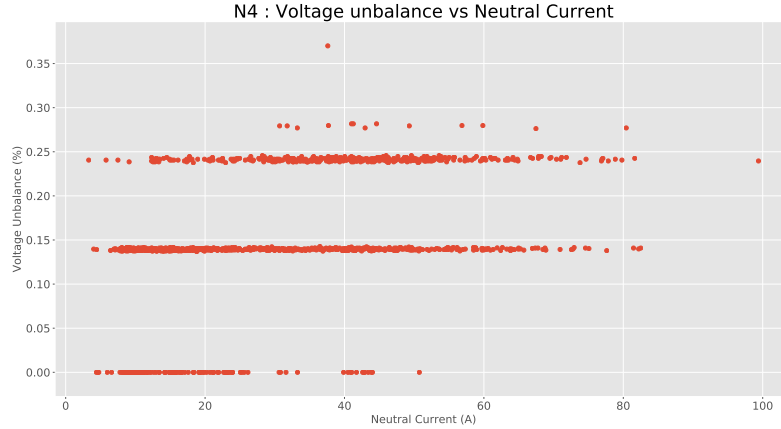


Figure 6.21: Voltage Unbalance vs Neutral Current N4

Figures 6.20 and 6.21 show the current and unbalanced current effect on the voltage level and voltage unbalance, respectively. Similarly to Network N3, there isn't a clear pattern between the phase voltage and current. However, it is possible to see a relation between the neutral current and voltage unbalance. However, the voltage unbalance is still very low.

6.5 Behaviour of the Networks

All networks, with the exception of Network N1, showed a reliable daily load pattern during the weekdays and the weekends. Networks N2, N3, and N4 showed a significantly smaller loading in the weekends. This could potentially limit the hosting capacity of PV.

The analysis of Network N2 showed a high capacitive power during the weekdays. Subsequently, if the active power demand from the utility side would drop, due to PV, the voltage might raise even more. Therefore, high capacitive power can limit the hosting capacity of PV as well.

During the weekdays, all main feeders' loading showed the highest load demands in the morning. This may limit the hosting capacity of EV charger systems. However, the high capacitive power of Network N2 can improve this.

Finally, the impedance characteristics of the networks were established. Network N3, which had the lowest transformer capacity had the highest network impedance, whereas Network N1 had the lowest network impedance. This is because the design of the network should maintain the nominal current flow.

Part III

Hosting Capacity Algorithm

Chapter 7

Hosting Capacity

7.1 Algorithm

The goal of the algorithm is to calculate hosting capacity, while considering the different behavioural characteristics of the network, PV System and EV Charger System. Figure 7.1 shows the flowchart of the proposed algorithm. Table 7.1 shows the inputs and outputs of the program, respectively.

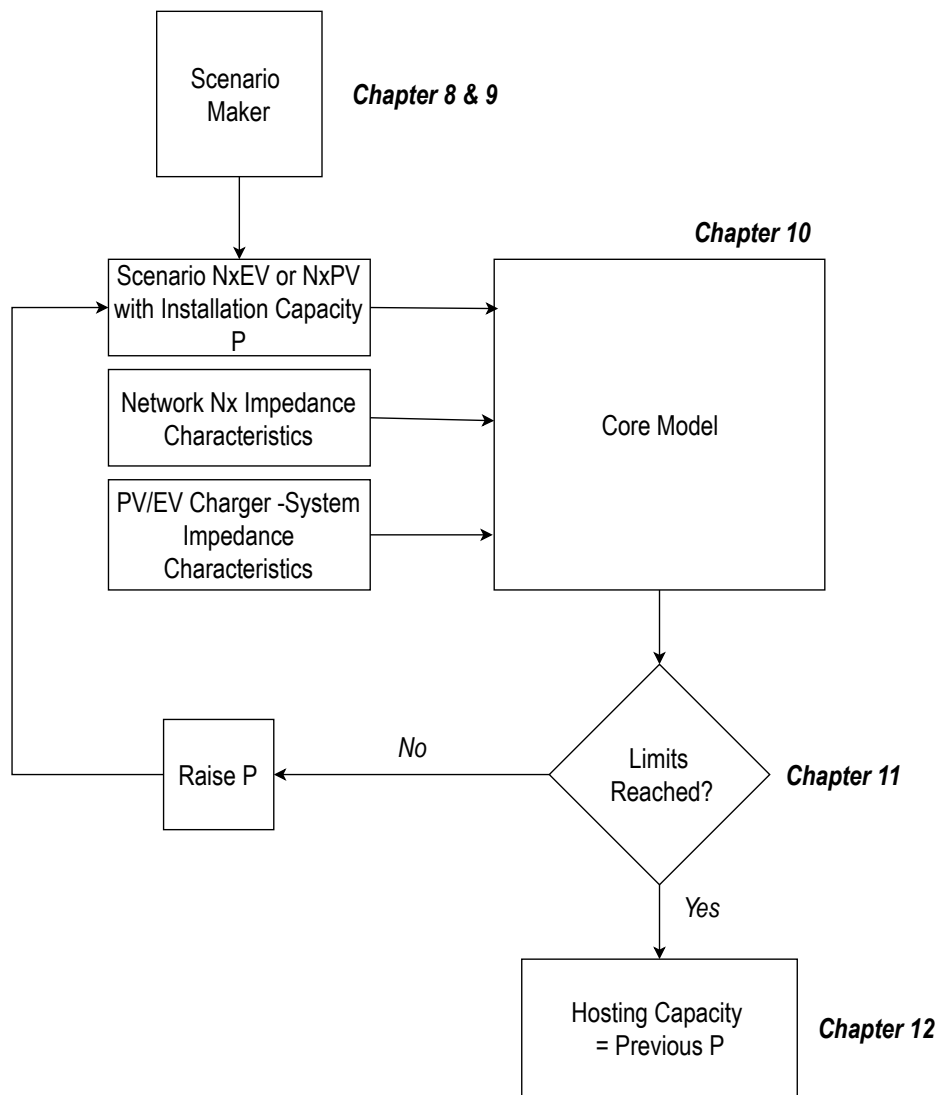


Figure 7.1: Pseudo-algorithm for calculating the hosting capacity of Network Nx.

Table 7.1: Aspects of the Algorithm.

Name	Description	Chapter
"Scenario Maker"	Desiscion algorithm that creates the worst case scenarios, NxPV and NxEV.	8 & 9
"Scenario NxEV ... Capacity P"	Scenarios NxPV and NxEV, containing the power behaviours of the network, and PV, or EV charger systems.	9
"Network ... Characteristics"	The impedance of network Nx.	/
"PV/EV ... Characteristics"	The impedance of PV, or EV charger system's feeder.	/
"Core Model"	The core model that calculates the slow voltage variations and voltage unbalances	10
"Limits Reached?"	Part of the algorithm that decides whether the voltage variations and unbalances have reached the predetermined limits.	11
"Raise P"	If limits aren't reached, installed capacity P is raised with a predetermined number.	/
"Hosting .. P"	The hosting capacity of PV or EV Charger system is the capacity P, from previous cycle.	12

The algorithm starts by importing the network's characteristics, and chosen scenarios for the utility voltage, network loading and either independent PV generation or EV charging. The choice for these scenarios and network characteristics are explained in chapter 8 and 9. These inputs are then used for the calculation of the voltage level and voltage unbalances in the network, in chapter 10. Afterwards, the results of the calculation are compared to the chosen limits, explained in chapter 11. If the limits aren't reached, the cycle starts over with a raised value of installed capacity of the PV, or EV charging scenario. Finally, if the limits are reached, the previous cycle's installed capacity, is saved as the hosting capacity for this input. The outcome of the algorithm is explained in Chapter 12.

Chapter 8

Scenario Models

8.1 PV System

8.1.1 PV Model

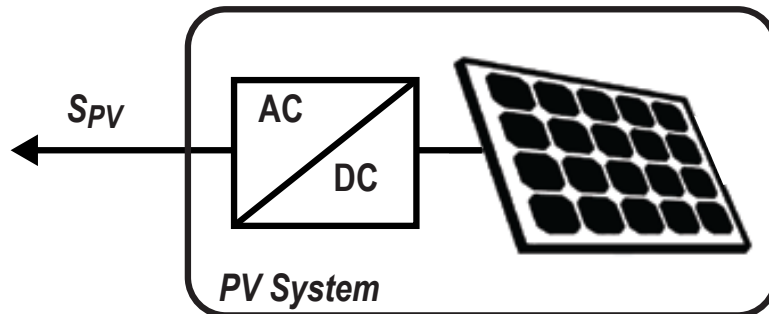


Figure 8.1: Output of the PV System

Figure 8.1 shows the output of the PV System. The PV system model generates a set of apparent power values, that represent this output. Moreover, it is assumed that the system's inverter operates at unity power factor, meaning that only active power is generated.

Equation 8.6 shows the formula for the active power output of a PV system, $P_{output}(t)$, in Watts. The equation was derived from Equations, 8.3 and 8.5, which represent the total irradiance on the module, $S_M(t)$ in Watts per square meter, and the temperature coefficient $c_T(t)$, respectively. These last two equations were extracted from [27].

Table 8.1: Input of the PV System Model

Input	Description	Unit
S_{DNI}	KNMI Direct Irradiance	W/m ²
S_{DHI}	KNMI Diffused Irradiance	W/m ²
A_s	KNMI Azimuth Angle	deg
a_s	KNMI Zenith Angle	deg
T_a	KNMI Temperature	C°
θ_M	PV Module Tilt	deg
A_M	PV Module Zenith Angle	deg
η_M	PV Module Efficiency	%
$\eta_{inverter}$	PV Inverter Efficiency	%
$Area$	PV Module Area	m ²
P_{Nom}	PV Module Nominal Power	Wp
T_{NOCT}	PV Nominal Operating Temperature	C°
Λ	PV Temperature Coefficient	%/C°
$P_{installed}$	PV Installed Capacity	Wp

Table 8.1 shows the inputs of the PV system model. The model requires weather station data, and PV system's characteristics. The weather station data is acquired from KNMI [28].

Calculate the solar irradiance on the module, $S_M(t)$:

$$S_{DNI_M}(t) = S_{DNI}(t) \cdot (\sin \theta_M \cdot \cos a_s(t) \cdot \cos(A_M - A_s(t)) + \cos \theta_M \cdot \sin a_s(t)) \quad (8.1)$$

$$S_{DHI_M}(t) = S_{DHI}(t) \left(\frac{1 + \cos \theta_M}{2} \right) \quad (8.2)$$

$$S_M(t) = S_{DHI_M}(t) + S_{DNI_M} \quad (8.3)$$

Calculate the total temperature coefficient, $c_T(t)$:

$$T_{Cell}(t) = T_a(t) + \frac{S_{module}(t)}{800} (T_{NOCT} - 20) \quad (8.4)$$

$$c_T(t) = 1 - \lambda(T_{cell}(t) - 25) \quad (8.5)$$

Calculate the output of the PV system, $P_{output}(t)$:

$$P_{output}(t) = S_{module}(t) \cdot \eta_M \cdot \eta_{inverter} \cdot c_T(t) \cdot Area \cdot \frac{P_{Installed}}{P_{Nom}} \quad (8.6)$$

8.1.2 Model vs Reality

In this example, the output of the model is compared to the real set of PV output from Chapter 4. The model input are the PV system characteristics from Table 4.1, an inverter efficiency of 95%, and KNMI weather data. The KNMI data that was utilized in this case, is the average recorded hourly irradiation and temperature data over the last 28 years [28]. This resulted in Figures 8.2 and 8.3.

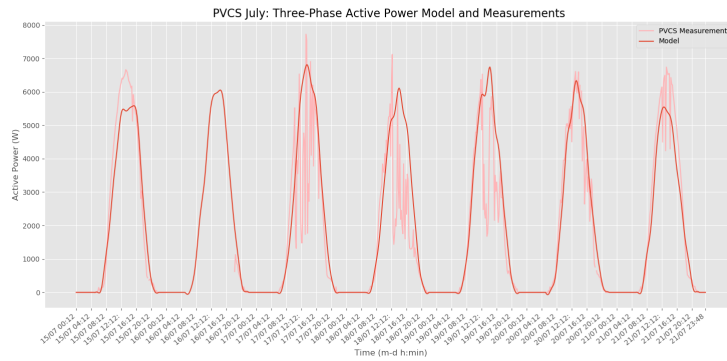


Figure 8.2: Model and Measurements comparison in July.

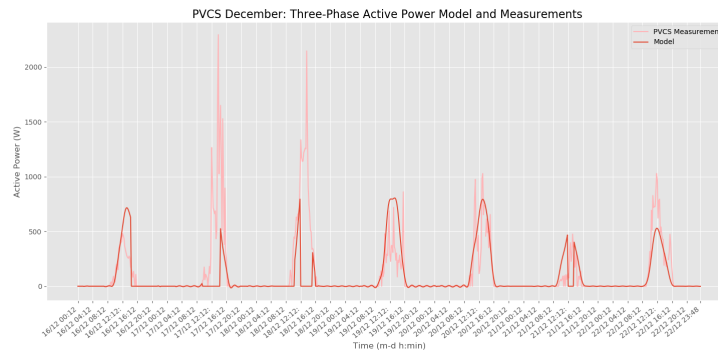


Figure 8.3: Model and Measurements comparison in December.

It seems that the combined KNMI data and model is less suited during cloudy conditions. This is shown by the lack of fast power deviations in both Figures 8.2 and 8.3. Cloud formation is harder to predict, which lead to a difference in solar irradiation incident, between the real and the average situation provided by KNMI.

On the other hand, by comparing the model and the outline of the measurements in Figure 8.2, it seems that model is capable of providing a realistic

PVS output during non or less cloudy conditions in July. This is especially useful in determining the maximum hosting capacity.

8.2 EV Charger System

8.2.1 EV Charger Model

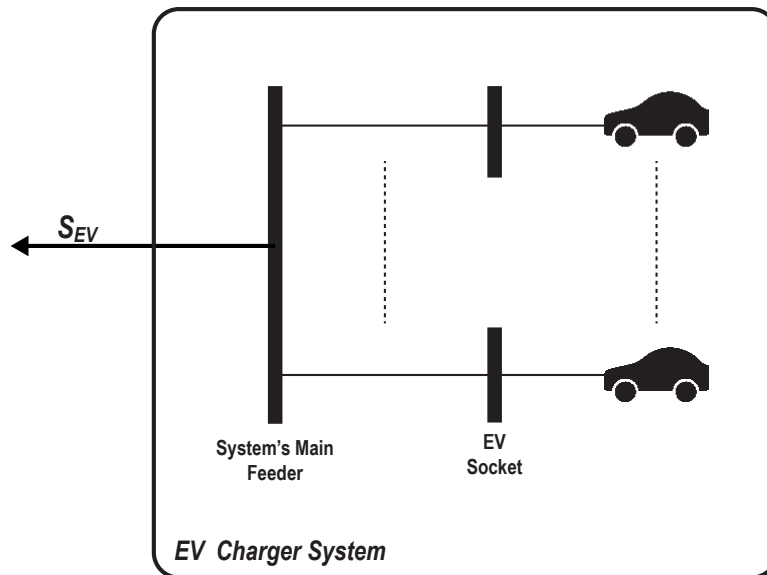


Figure 8.4: The output of the EV charger system. Mind that the charger system is drawing power from the network.

Figure 8.4 shows the output of the EV Charger system. The EV charger system model creates a set of apparent power values that represent the daily output. Similarly to the PV system, it is assumed that the EV charger system has a unity power factor.

Equations 8.7-8.9 represent the equations for the daily power output, $P_{EVCS}(t)$. These equations were derived from the measurements presented in Chapter 5.

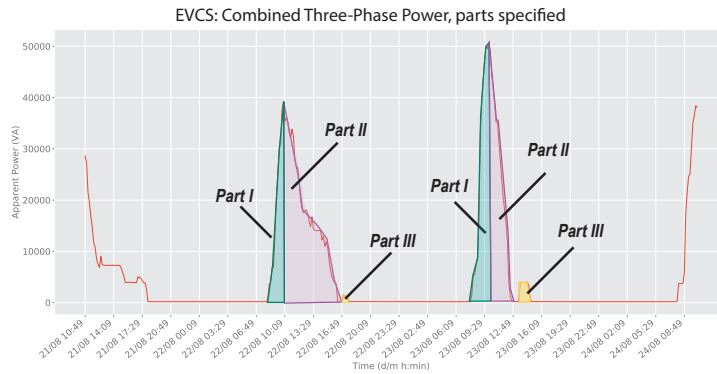


Figure 8.5: The power measured at the EV Charging System of Chapter 5, with parts specified.

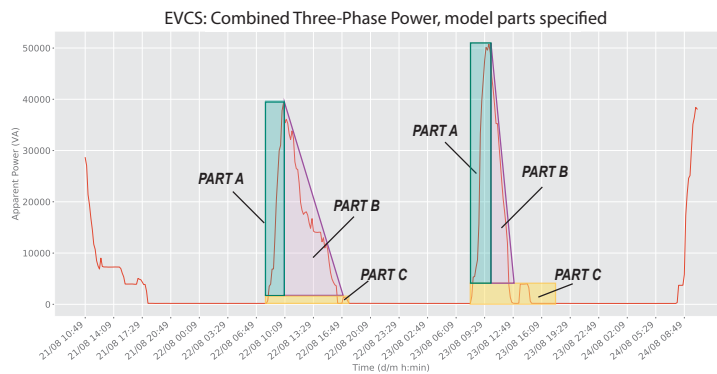


Figure 8.6: The proposed model behaviour of the system

Figure 8.5 represents the total power output of the EV charger system, as presented in Chapter 5, with three parts specified. The first part (I) is the simultaneous connection and charging during the morning. Here, the power quickly increases, and then flattens. In the afternoon, part (II), the power drops. Here, more EVs are disconnecting than connecting. The last part (III), represents the postponed connection of EVs due to unavailable chargers during the day.

The proposed model of the EV Charger system behaviour is presented in Figure 8.6. The proposed behaviour leads to Equations 8.7-8.9. The part that represents the increase and flattening of the power behaviour is summarized as part A. Similarly to part (II), part B represents the decrease in power. Finally, part C represents the constant available power.

For t_{start} , and the end time, t_{end} . $t_{B_{start}}$ and $t_{B_{end}}$ are the start end end times of part B.

$$P_{EVCS}(t) = a + c$$

$$\text{For } t_{start} < t < t_{B_{start}} \quad (8.7)$$

$$P_{EVCS}(t) = a + c - \frac{a}{t_{B_{end}} - t_{B_{start}}} \cdot (t - t_{B_{start}})$$

$$\text{For } t_{B_{start}} < t < t_{B_{end}} \quad (8.8)$$

$$P_{EVCS}(t) = c$$

$$\text{For } t_{B_{end}} < t < t_{end} \quad (8.9)$$

8.2.2 Model vs Reality

Table 8.2: Input of the EV Charger model's equations.

Name	Value	
	Day 2	Day 3
$a + c$	40 kVA	51kVA
c	1.5 kVA	4 kVA
t_{start}	8:09	7:59
t_{end}	17:49	15:09
$t_{B_{start}}$	10:09	10:09
$t_{B_{end}}$	16:49	13:09

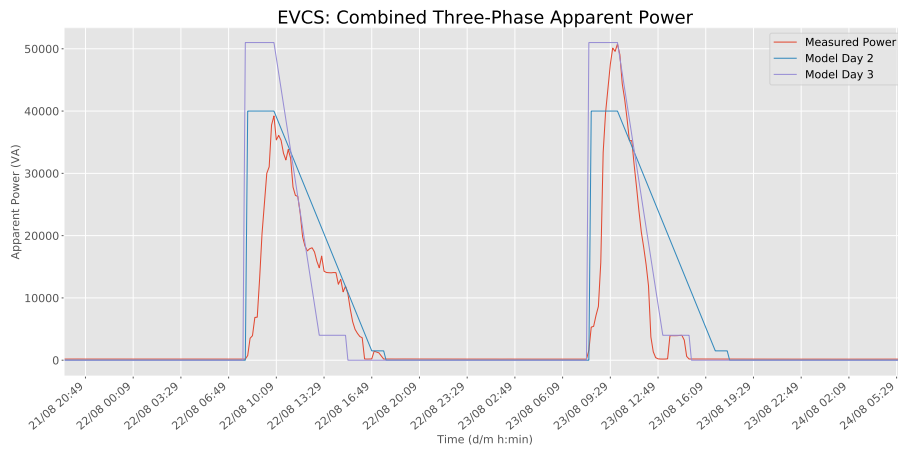


Figure 8.7: The modelled outputs versus the measurements.

Figure 8.7 shows the measured power from chapter 5, the model based on the second day and the model based on the third day. Table shows the input values for the Equations 8.7-8.9. The day 2 model uses a total energy of 208.8 kWh, whereas day 3 model has a total energy of 189 kWh.

8.3 Utility Voltage

8.3.1 Utility Voltage Model

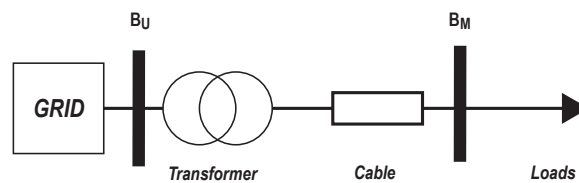


Figure 8.8: One-line diagram of the network with named buses. Based on Figure 6.1

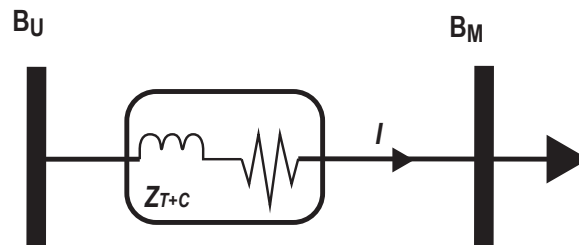


Figure 8.9: Simplification of Figure 8.8

Figures 8.8 and 8.9 show the configurations of the network, which are based on the measurement configuration in Chapter 6. Thus, the calculation of the utility voltage is based on the networks' measurements.

Equation 8.12 shows the equation for the utility voltage $U_{LxU}(t)$, for a network with a three-phase voltage, $U_M(t)$, and a three-phase apparent power, $S_M(t)$. This is derived from Equations 8.10- 8.11. Finally, Table 8.3 shows the inputs.

Table 8.3: Inputs of the Utility voltage's model equations.

Input	Description	Unit
U_{L1M} U_{L2M} U_{L3M}	The three-phase voltages, measured at the main feeder.	V
Z_{T+C}	The combined transformer and cable impedance in the network.	Ω
S_{L1M} S_{L2M} S_{L3M}	The Three-Phase apparent powers measured at the main feeder.	VA

For Phase Lx in Phases $L1, L2, L3$:

The utility voltage is equal to the sum of the main feeder's voltage and in-between voltage drop:

$$U_{LxU}(t) = \Delta U + U_{LxM}(t) \quad (8.10)$$

Using Ohm's Law, $U = I \cdot Z$:

$$U_{LxU}(t) = Z_{T+C} \cdot I + U_{LxM}(t) \quad (8.11)$$

Using Power Law, $S = U \cdot I^$:*

$$U_{LxU}(t) = Z_{T+C} \left(\frac{S_{LxM}(t)}{U_{LxM}(t)} \right)^* + U_{LxM}(t) \quad (8.12)$$

8.3.2 Model vs. Reality

Table 8.4: Input values of Equation 8.12

Name	Value
U_{L1M}	Three-phase voltages of Network N1
U_{L2M}	
U_{L3M}	
Z_{T+C}	Impedance of N1 from Table 6.3
S_{L1M}	Three-Phase Active and Reactive Powers of Network N1
S_{L2M}	
S_{L3M}	

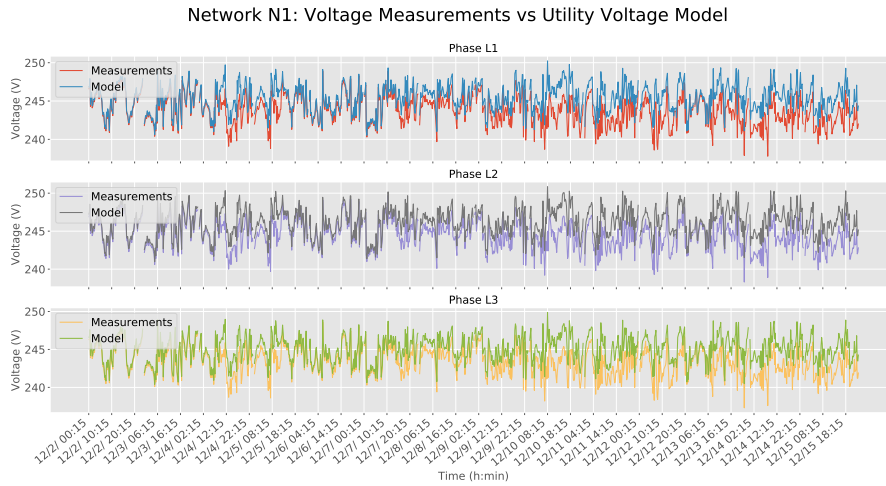


Figure 8.10: The voltage measurements from Chapter 6, and the modelled utility voltage.

Table 8.5: Range of the Utility Voltage.

Phase	Max	Min	Difference	Percentage Nominal
L1	250.3	240.6	9.7	4.2%
L2	250.9	241.0	9.9	4.3%
L3	249.9	240.5	9.4	4.1%

Figure 8.10 shows the modelled voltages and the measured voltages of Network N1. Table 8.5 shows the range of the modelled voltages. The measured voltages are the voltages at the main feeder, as described in Chapter 6, since

there are no measurements of the actual utility voltage. Subsequently, a difference between the modelled voltages and measured voltages is expected.

The three-phase utility voltage difference is 9.7, 9.9, and 9.4, which is between 4.1% and 4.3% of the nominal voltage of 230V. On average, the utility voltage is 15 V higher than the nominal voltage. It is likely that this is due to the transformer's tap settings. As expected, the difference between the voltage measurements and the utility voltage is related to the active and reactive power measurements shown in Figure 6.2.

Chapter 9

Scenarios

9.1 The Scenario Maker

The goal of the scenario maker is to create and combine 'worst' case subscenarios for PV generation, EV charging, network loading and utility voltage. Figure 9.1 shows which worst case subscenarios combine to create the worst case scenarios NxPV, and NxEV, for a Network Nx. Subsequently, each network has two different scenarios that represent the worst case situations for PV generation and EV Charging.

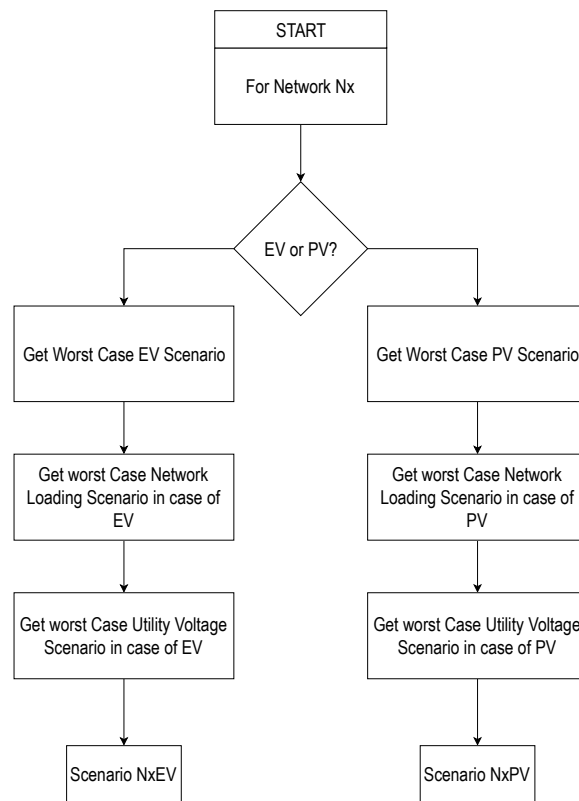


Figure 9.1: Operation of the scenario maker.

9.2 Worst Case PV Subscenario

Figure 9.2 shows the extreme case PV subscenario, utilized for calculating the hosting capacity of a PV system.

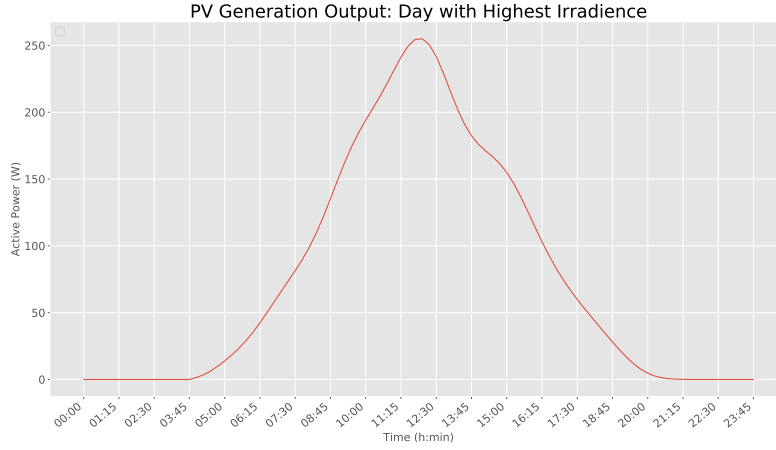


Figure 9.2: Output of the PV Subscenario.

Table 9.1: PV System Characteristics

Input	Value
θ_M	28 °
A_m	180 °
η_M	22.6 %
Area	1.690*1.046 m ²
P_{Nom}	400 Wp
T_{NOCT}	45°C
λ	-0.29%/°C
$\eta_{inverter}$	99.2%

PV generation may risk overvoltage and unbalances by injecting too much current into the network. Since PV generation is related to the amount of solar irradiance, the highest PV generation is expected on a clear sunny day. The data used for finding the highest irradiance is extracted from KNMI. This datasheet shows the hourly average over one year, based on 28 years weather data.

Table 9.1 shows the PV characteristics of a PV system with an installed capacity of 400 Wp. In the Netherlands, for generating maximum power, the optimal tilt is 28 degrees, and the most optimal azimuth angle is 180 degrees [29]. The PV module characteristics are based on the highest efficiency module on the market, according to [30]. The nominal operating temperature of the module is unknown. Therefore, a T_{NOCT} of 45°C is assumed.

Recent commercial large scale inverters have efficiencies up to 99.2% [31]. Additionally, the PV system is wired three-phase, meaning that each phase

injects equal amount of power.

9.3 Worst Case EV Subscenario

Figure 9.3 shows the extreme case EV Charging Subscenario. EV charging may risk undervoltages and unbalances by drawing too much current from the network. As shown in Chapter, there are different behaviours possible for the same installation. The subscenario with the highest power is subscenario day 3. Finally, in the worst case scenario, all EVs draw power singularly from Phase L1. The installed capacity is the maximum power drawn.

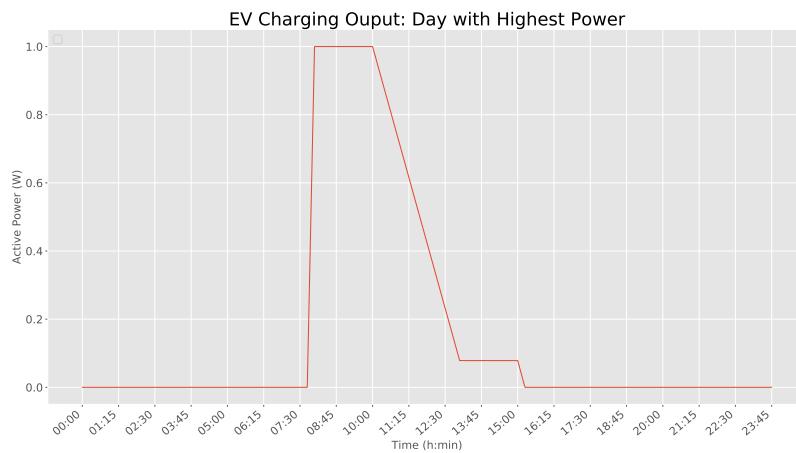


Figure 9.3: Output of the EV Charging Subscenario.

9.4 Worst Case Network Subscenario

Figures 9.4 and 12.9 show the extreme case network subscenarios of Network N1, for PV generation and EV charging, respectively. The worst case network loading scenario for PV generation is the day where the active and reactive power demand lead the least, or most negative voltage drop, while the PV system is generating. On the other hand, the worst network scenario for EV charging, is when the active and reactive power demand lead to the highest voltage drop at the main feeder, while the EVs are charging.

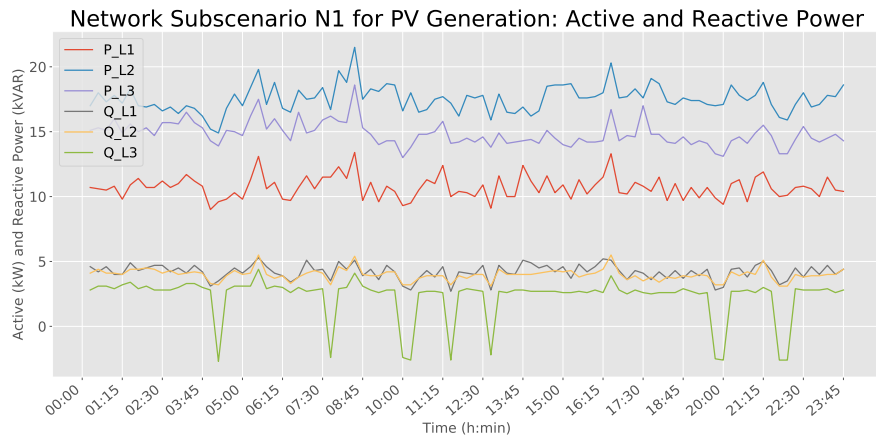


Figure 9.4: Loading of Network N1 during the PV Generation Subscenario.

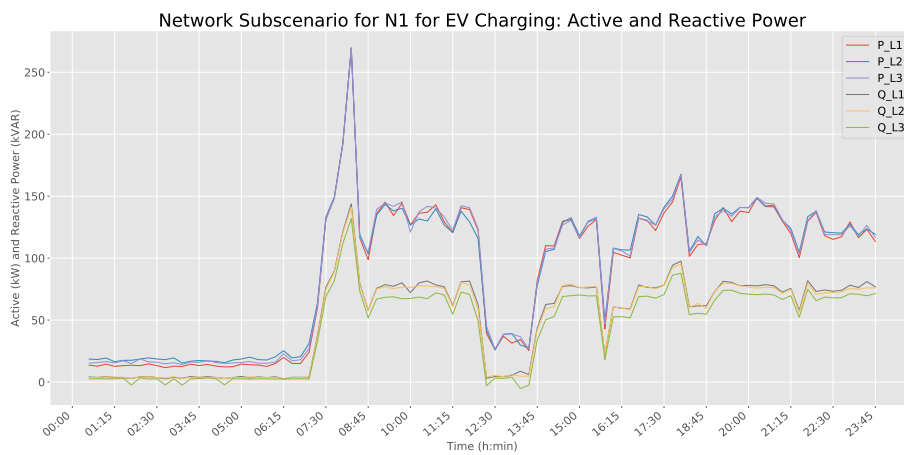


Figure 9.5: Loading of Network N1 during the EV Charging Subscenario.

9.5 Worst Case Utility Voltage Subscenario

Figure 9.6 shows the extreme case utility voltage subscenario for PV generation and EV charging.

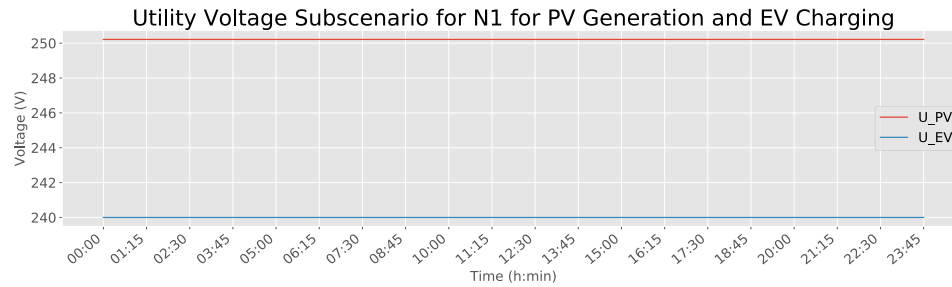


Figure 9.6: Three-phase voltage during the EV Charging Subscenario.

The highest and lowest utility voltages are the worst case utility voltages for PV generation, and EV charging, respectively. This is because these utility voltages provide the biggest risks for creating overvoltages and undervoltages, respectively. Moreover, unlike the other subscenarios, the worst case utility voltages are kept constant during the entire scenario.

Chapter 10

Core Model

10.1 Input and Outputs

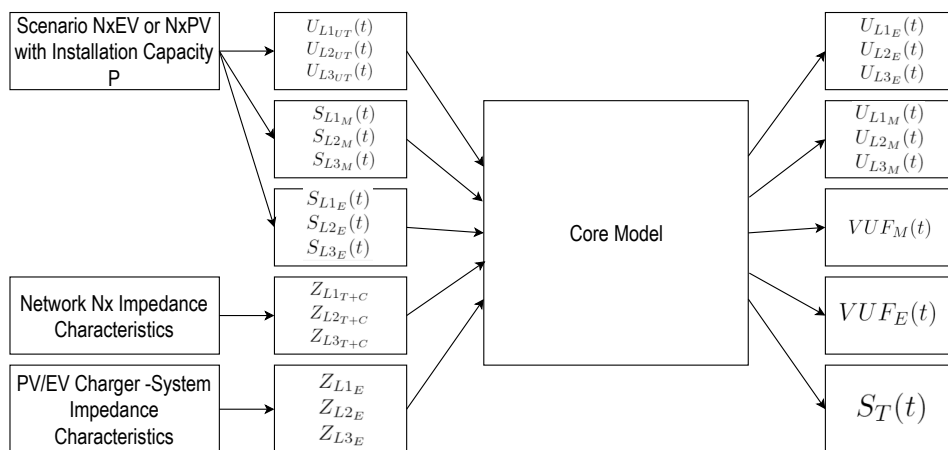


Figure 10.1: Input and output diagram of the Core Model.

Table 10.1: Core Model's inputs

Inputs	Symbol	Unit
Utility Phase Voltages	$U_{L1_{UT}}(t)$ $U_{L2_{UT}}(t)$ $U_{L3_{UT}}(t)$	V
Network Loading	$S_{L1_M}(t)$ $S_{L2_M}(t)$ $S_{L3_M}(t)$	VA
Extension Loading, or Generation	$S_{L1_E}(t)$ $S_{L2_E}(t)$ $S_{L3_E}(t)$	VA
Transformer, and Cable Impedance	$Z_{L1_{T+C}}$ $Z_{L2_{T+C}}$ $Z_{L3_{T+C}}$	Ω
Extension Cable Impedance	Z_{L1_E} Z_{L2_E} Z_{L3_E}	Ω

Table 10.2: Core Model's outputs

Outputs	Symbol	Unit
Main Feeder Phase Voltages	$U_{L1_M}(t)$ $U_{L2_M}(t)$ $U_{L3_M}(t)$	V
Extension Phase Voltages	$U_{L1_E}(t)$ $U_{L2_E}(t)$ $U_{L3_E}(t)$	V
Main Feeder Voltage Unbalance	$VUF_M(t)$	%
Extension Voltage Unbalance	$VUF_E(t)$	%
Transformer Total Loading	$S_T(t)$	VA

Figure 10.1 shows the placement of the equations within the program. Tables 10.1 and 10.2 describes the input and outputs of the core model.

10.2 Core Model Explanation

10.2.1 Present Situation

The present situation represents a network where EVCS and PVS have yet to be installed. A single line diagram of this situation is shown in Figure 10.2. This single line was inspired by the single line configuration in Chapter 6.

The Figure shows where the modelled part of the network starts. From left to right, the diagram consists of the grid, a transformer, a cable impedance and a load.

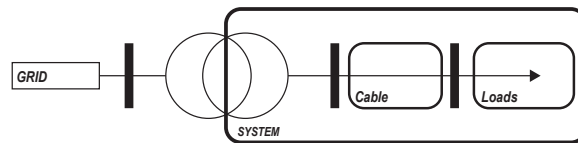


Figure 10.2: Single line diagram of the present situation where EVCS and PVS have yet to be installed.

The secondary side of the transformer is Wye grounded. The complete installation contains at least five wires, in which the first three represent the three phases L1, L2 and L3, and finally a neutral, and ground wire. Figure 10.3 represents the system in this Wye-connection.

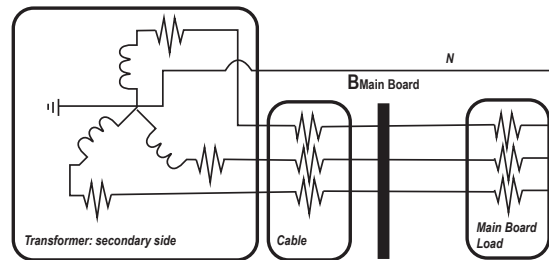


Figure 10.3: Three-phase circuit diagram of the present situation where EVCS and PVS have yet to be installed.

This three-phase circuit is simplified by separating it into three single phase systems, which is shown in Figure 10.4. The primary side of the transformer is modelled as a voltage source. The transformer and line impedance are summed. Finally, the load is modelled as a constant power load.

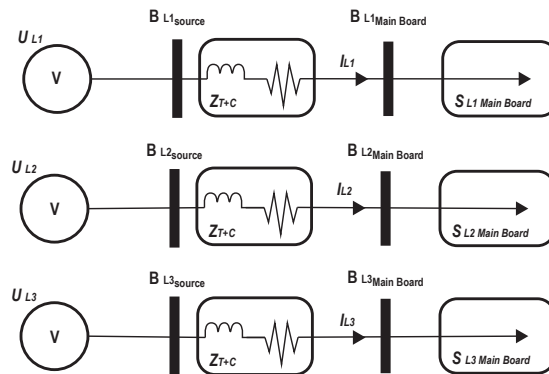


Figure 10.4: Three single phase diagrams: a simplification of Figure 10.3.

10.2.2 New Situation

The new situation represents the network with an extension added to the main feeder. This is shown in Figure 10.5. Subsequently, the three phase simplification is illustrated in Figure 10.6. The configuration of the PV and EV charger system are inspired by the configurations from Chapter 4 and 5.

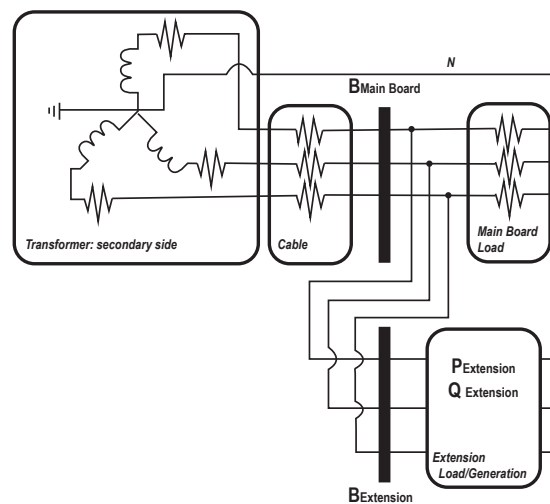


Figure 10.5: Three-phase circuit diagram of the new situation where EVCS or PVS have been installed.

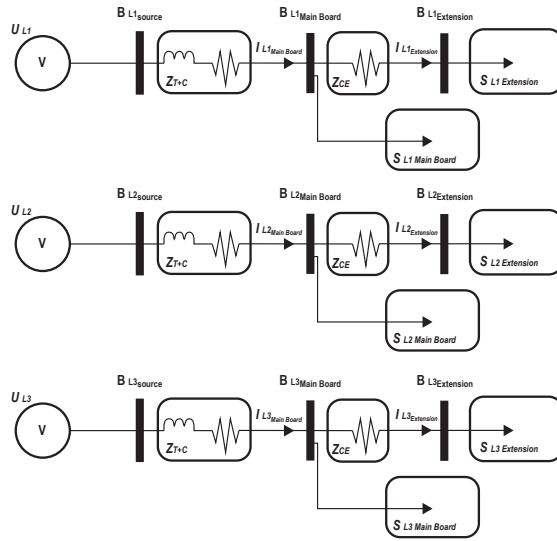


Figure 10.6: Three single phase diagrams of the new situation where PVS or EVCS has been added to the network.

10.3 Core Model Equations

10.3.1 Load-Flow Equations

Equations 10.11-10.10 are utilized to calculate the phase voltages at the main feeder, U_{L1M} , U_{L2M} , U_{L3M} , and at the extension, U_{L1E} , U_{L2E} , U_{L3E} . These Equations were derived from Equations 10.1 - 10.6.

The equations in each of the three phases are the same. Firstly, Kirchoff's current law is used to determine the currents at each node, B_M , and B_E . Then, Ohm's law is used to rewrite the currents in their respective voltages, U_M and U_E , and impedances, Z_{T+C} and Z_E . Using the electric power law, the apparent power at each node is determined. Then, the apparent powers at each bus are rewritten as the active and reactive power. The direction of the power relative to the node determines the polarity of the power. For example, if the power leaves the node, the polarity of the power is negative.

Subsequently, the end results of this derivation are four equations for P_M , P_E , Q_M , and Q_E , and four unknowns, $|U_M|$, $|U_E|$, $\delta_{\bar{U}_M}$ and $\delta_{\bar{U}_E}$, which are the nodes' voltage magnitudes and phases, respectively. These equations are solved by using the fsolve function in Python [32]. The resulting voltage magnitudes, and their respective phases, represent the phasor voltages at each node.

For Phase Lx in Phases $L1$, $L2$, $L3$:

Using Kirchoff's Current Law:

$$\bar{I}_{Lx_{SM}}(t) = \bar{I}_{Lx_{BM} \rightarrow Lx_{BUT}}(t) + \bar{I}_{Lx_{BM} \rightarrow Lx_{BE}}(t) \quad (10.1)$$

$$\bar{I}_{Lx_{SE}}(t) = \bar{I}_{Lx_{BE} \rightarrow Lx_{BM}}(t) \quad (10.2)$$

Using Ohm's Law: $U = I \cdot Z$

$$\bar{I}_{Lx_{SM}}(t) = \frac{\bar{U}_{Lx_M}(t) - \bar{U}_{Lx_{UT}}(t)}{\bar{Z}_{T+C}} + \frac{\bar{U}_{Lx_M}(t) - \bar{U}_{Lx_E}(t)}{\bar{Z}_E} \quad (10.3)$$

$$\bar{I}_{Lx_{SE}}(t) = \frac{\bar{U}_{Lx_E}(t) - \bar{U}_{Lx_M}(t)}{\bar{Z}_E} \quad (10.4)$$

Using Power Law: $S = U \cdot I^*$ [33]

$$\bar{S}_M(t) = \bar{U}_{Lx_M}(t) \cdot \bar{I}_{Lx_{SM}}(t)^* \quad (10.5)$$

$$= \bar{U}_{Lx_M}(t) \cdot \left(\frac{\bar{U}_{Lx_M}(t) - \bar{U}_{Lx_{UT}}(t)}{\bar{Z}_{T+C}} + \frac{\bar{U}_{Lx_M}(t) - \bar{U}_{Lx_E}(t)}{\bar{Z}_E} \right)^* \quad (10.6)$$

$$\bar{S}_E(t) = \bar{U}_{Lx_E}(t) \cdot \bar{I}_{Lx_{SE}}(t)^* \quad (10.7)$$

$$= \bar{U}_{Lx_E}(t) \cdot \left(\frac{\bar{U}_{Lx_E}(t) - \bar{U}_{Lx_M}(t)}{\bar{Z}_E} \right)^* \quad (10.8)$$

The Apparent power at each node can be rewritten as the active and reactive power at each node. [33]

$$\begin{aligned} P_{Lx_M}(t) &= \frac{|\bar{U}_{Lx_M}(t)|^2}{\bar{Z}_{T+C}} \cdot \cos(\theta_{\bar{Z}_{T+C}}) \\ &\quad - \frac{|\bar{U}_{Lx_M}(t)| |\bar{U}_{Lx_{UT}}(t)|}{|\bar{Z}_E|} \cdot \cos(\theta_{\bar{Z}_{T+C}} + \delta_{\bar{U}_{Lx_M}}(t) - \delta_{\bar{U}_{Lx_E}}(t)) \\ &\quad + \frac{|\bar{U}_{Lx_M}(t)|^2}{|\bar{Z}_E|} \cdot \cos(\theta_{\bar{Z}_E}) \\ &\quad - \frac{|\bar{U}_{Lx_M}(t)| |\bar{U}_{Lx_E}(t)|}{|\bar{Z}_E|} * \cos(\theta_{\bar{Z}_E} + \delta_{\bar{U}_{Lx_M}}(t) - \delta_{\bar{U}_{Lx_E}}(t)) \end{aligned}$$

(10.9)

$$\begin{aligned}
Q_{Lx_M}(t) &= \frac{|\bar{U}_{Lx_M}(t)|^2}{\bar{Z}_{T+C}} \cdot \sin(\theta_{\bar{Z}_{T+C}}) \\
&\quad - \frac{|\bar{U}_{Lx_M}(t)||\bar{U}_{Lx_{UT}}(t)|}{|\bar{Z}_E|} \cdot \sin(\theta_{\bar{Z}_{T+C}} + \delta_{\bar{U}_{Lx_M}}(t) - \delta_{\bar{U}_{Lx_E}}(t)) \\
&\quad + \frac{|\bar{U}_{LxB_M}(t)|^2}{|\bar{Z}_E|} \cdot \sin(\theta_{\bar{Z}_E}) \\
&\quad - \frac{|\bar{U}_{Lx_M}(t)||\bar{U}_{Lx_E}(t)|}{|\bar{Z}_E|} \cdot \sin(\theta_{\bar{Z}_E} + \delta_{\bar{U}_{Lx_M}}(t) - \delta_{\bar{U}_{Lx_E}}(t))
\end{aligned} \tag{10.10}$$

$$\begin{aligned}
P_{Lx_E}(t) &= \frac{|\bar{U}_{Lx_E}(t)|^2}{|\bar{Z}_E|} \cdot \cos(\theta_{\bar{Z}_E}) \\
&\quad - \frac{|\bar{U}_{Lx_E}(t)||\bar{U}_{LxB_M}(t)|}{|\bar{Z}_E|} \cdot \cos(\theta_{\bar{Z}_E} + \delta_{\bar{U}_{Lx_E}}(t) - \delta_{\bar{U}_{Lx_M}}(t))
\end{aligned} \tag{10.11}$$

$$\begin{aligned}
Q_{Lx_E}(t) &= \frac{|\bar{U}_{Lx_E}(t)|^2}{|\bar{Z}_E|} \cdot \sin(\theta_{\bar{Z}_{CE}}) \\
&\quad - \frac{|\bar{U}_{Lx_E}(t)||\bar{U}_{Lx_M}(t)|}{|\bar{Z}_E|} \cdot \sin(\theta_{\bar{Z}_E} + \delta_{\bar{U}_{Lx_E}}(t) - \delta_{\bar{U}_{Lx_M}}(t))
\end{aligned} \tag{10.12}$$

By solving the four load equations, the voltages at each bus are determined.

$$\bar{U}_{Lx_E} = |\bar{U}_{Lx_E}(t)| \angle \delta_{\bar{U}_{Lx_E}} \tag{10.13}$$

$$\bar{U}_{Lx_M} = |\bar{U}_{Lx_M}(t)| \angle \delta_{\bar{U}_{Lx_M}} \tag{10.14}$$

10.3.2 Voltage Unbalance

The voltage unbalances, at each node, VU_M and VU_E , are calculated by using the IEC definition for voltage unbalance VU , as described in Chapter 2.

10.3.3 Transformer Total Load

The total loading of the transformer is calculated according to Equations 10.15 and 10.16.

For Phase Lx in Phases $L1, L2, L3$:

$$\bar{I}_{LxT} = \bar{I}_{LxB_{UT} \rightarrow B_M} \quad (10.15)$$

$$S_T = \sum_{x=1}^3 \bar{U}_{LxUT} \cdot \bar{I}_{LxT} \quad (10.16)$$

Chapter 11

Limits

Figure 11.1 shows the voltage and voltage unbalance limits, which are evaluated in the framework. Table 11.1 shows the descriptions of the illustrated limits.

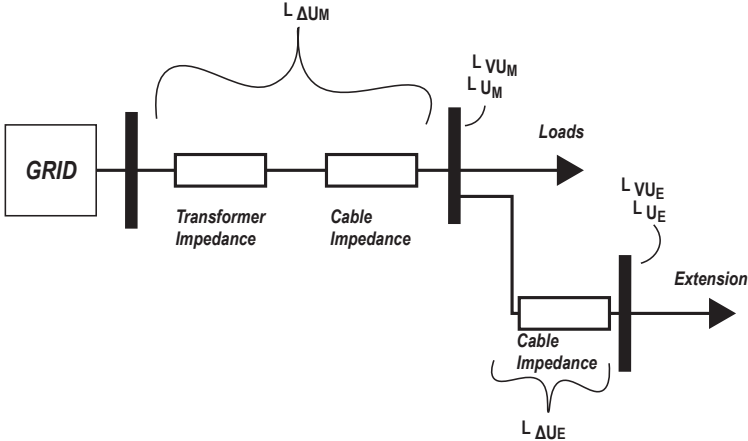


Figure 11.1: Voltage and Voltage unbalance limits in relation to the analyzed network.

Table 11.1: Descriptions of the limits

Name	Description
$L_{\Delta U_M}$	Limit for voltage drop over the transformer and cable impedance
L_{U_M}	limits for the maximum and minimum voltage level at the main feeder
L_{VU_M}	Limit for the voltage unbalance at the main feeder.
$L_{\Delta U_E}$	Limit for voltage drop over the extension's cable impedance
L_{U_M}	limits for the maximum and minimum voltage level at the extension's feeder
L_{VU_E}	Limit for the voltage unbalance at the extension's feeder.



11.1 PV System

Table 11.2 shows the limits for the PV system, which were used for calculating the hosting capacity.

Table 11.2: limits for the PV system.

Input	Name	Values
$L_{\Delta U_E}$	$L_{\Delta U_{PV}}$	1%
L_{U_E}	$L_{U_{PV}}$	184V - 253V
L_{VU_E}	$L_{VU_{PV}}$	2%

The suggested voltage drop Limit between the start of the installation and the PV installation is 1% [34]. For PV systems of every size, the inverter must trip at a voltage equal to or higher than 253 V for 2 seconds. Additionally, the system must trip at a voltage equal to or lower than 184 V for 2 seconds [15]. In case of a load imbalance, most standards set a general limit of 2% for the PV system voltage unbalances [35].

11.2 EV Charger System

Table 11.3: limits for the EV system.

Input	Name	Values
$L_{\Delta U_E}$	$L_{\Delta U_{EV}}$	1%
L_{U_E}	$L_{U_{EV}}$	207V - 253V
L_{VU_E}	$L_{VU_{EV}}$	2%

As stated in Chapter 2, the voltage drop, between the start of the installation and the load, should be no more than 5% of the nominal voltage. However, the EV charger installation consists of a main feeder, and a socket, to which the EV, the final load, is connected. Therefore, this voltage drop must be taken into account, not only up to EV charger installation, but also inside the installation. As there were no suggested voltage drops between the main feeder and the EV charger installation available to the author, it was decided to estimate the maximum voltage drop with a thought experiment.

Especially for large EV charger installations, with many separate car charging points, the total car park can take up a lot of space. Then, it would be suggested to leave a voltage drop range, for the connection of the sockets, that takes up the majority of the maximum allowed voltage drop. Therefore, the maximum voltage drop up to the EV charger system is 1%.

Finally, as stated in Chapter 2, the IEC suggest a voltage range between 207V and 253V for devices. For the voltage unbalance, an unbalance limit of no more than 2% is advised. The limits are summerized in Table 11.3

11.3 Network

For the rest of the network, the same limits as discussed in Chapter 2 are used. These are shown in Table 11.4.

Table 11.4: limits of the network

Input	Values
$L_{\Delta U_M}$	3%
L_{U_M}	207V - 253V
L_{VU_M}	2%

Chapter 12

Outcome of the Algorithm

12.1 Background

In this chapter, the hosting capacity was calculated for four different networks, using the proposed algorithm as explained in Chapter 7. Subsequently, the outcome of the algorithm was analyzed on its performance. The networks of which the hosting capacity was calculated are the same networks from Chapter 6. Firstly, the exact input of the algorithm is described. Then, the outcome of the algorithm is plotted.

12.2 Algorithm Input

12.2.1 Network Impedance and limits

The network impedances are drawn from Table 6.3. Furthermore, the limits, as described in Chapter 11, are used.

12.2.2 Scenarios

Using the Scenario Maker, for every network, two scenarios, that represent the worst case situation for either PV generation, or EV Charging, were created out of multiple subscenarios.

Scenario N1PV and N1EV

Table 12.1: Utility Voltage Subscenario for N1

Scenario	Voltage (V)
N1PV	250.2
N1EV	240.0

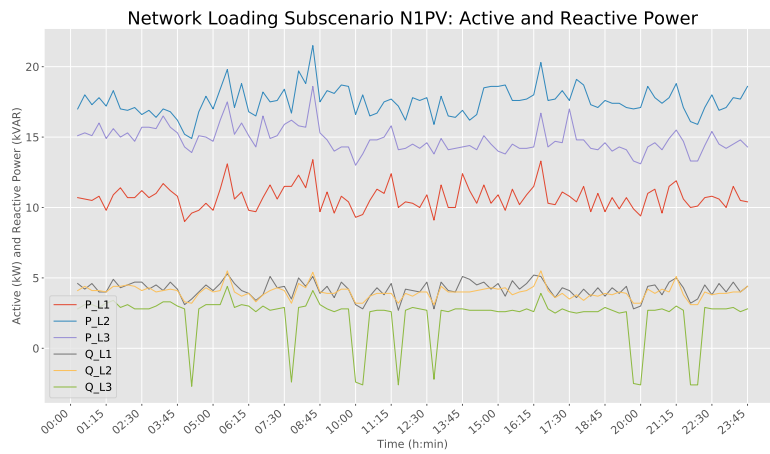


Figure 12.1: Network Subscenario for Scenario N1PV

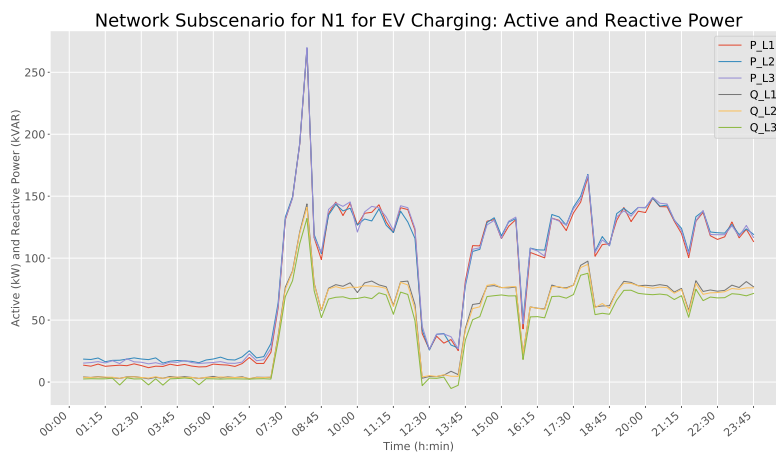


Figure 12.2: Network Subscenario for Scenario N1EV

Scenario N2PV and N2EV

Table 12.2: Utility Voltage Subscenario for N2

Scenario	Voltage (V)
N2PV	249.1
N2EV	238.6

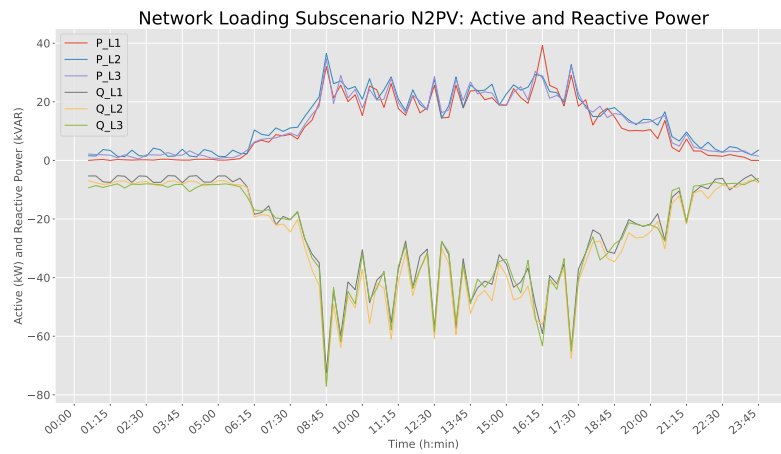


Figure 12.3: Network Subscenario for Scenario N2PV

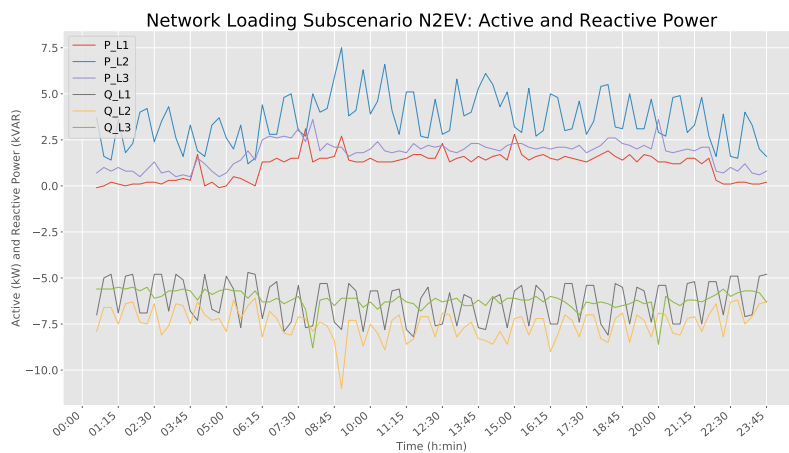


Figure 12.4: Network Subscenario for Scenario N2EV

Scenario N3PV and N3EV

Table 12.3: Utility Voltage Subscenario for N3

Scenario	Voltage (V)
N3PV	246.4
N3EV	233.9

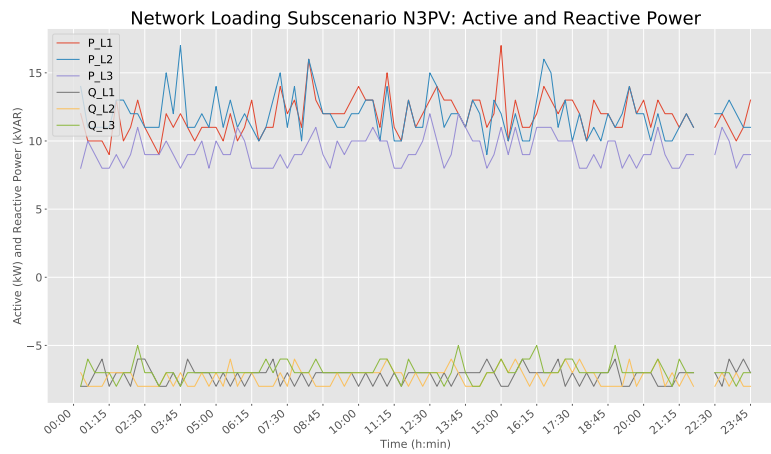


Figure 12.5: Network Subscenario for Scenario N3PV

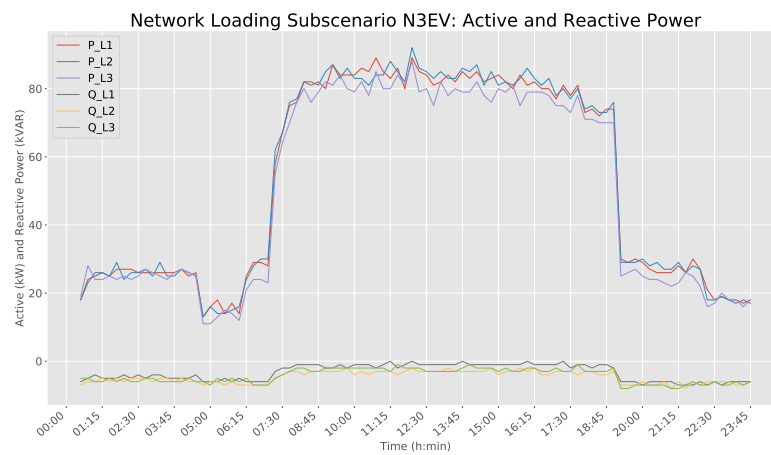


Figure 12.6: Network Subscenario for Scenario N3EV

Scenario N4PV and N4EV

Table 12.4: Utility Voltage Subscenario for N4

Scenario	Voltage (V)
N4PV	246.2
N4EV	234.1

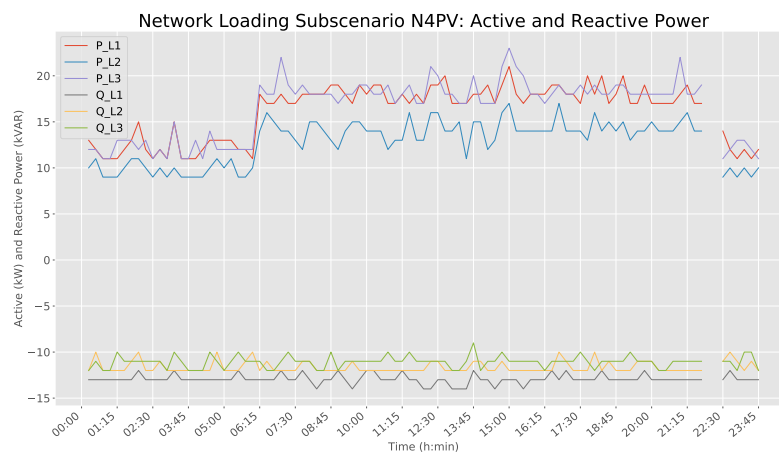


Figure 12.7: Network Subscenario for Scenario N4PV

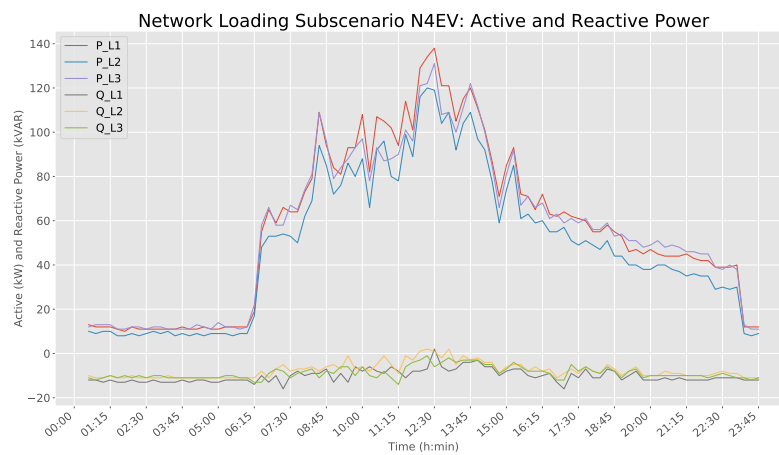


Figure 12.8: Network Subscenario for Scenario N4EV

12.2.3 PV or EV Charging System feeder impedance

The hosting capacity was calculated for a range of PV or EV charger system's feeder's resistances, in ohms. The chosen range is explained in Equation 12.2.

For $0 < n < 45$:

$$R_E = \frac{1.2^n}{1000} \quad (12.1)$$

12.2.4 Installed Capacity P

As explained in Equation 12.2, for every cycle, the installed capacity P, in Watts, was raised with steps of 10 kW. This cycle went up to the maximum capacity of the transformer.

For $0 < n < \frac{\text{Transformer Capacity}}{10000}$:

$$P = 10000 \cdot n \quad (12.2)$$

12.3 Algorithm Output

12.3.1 Network N1

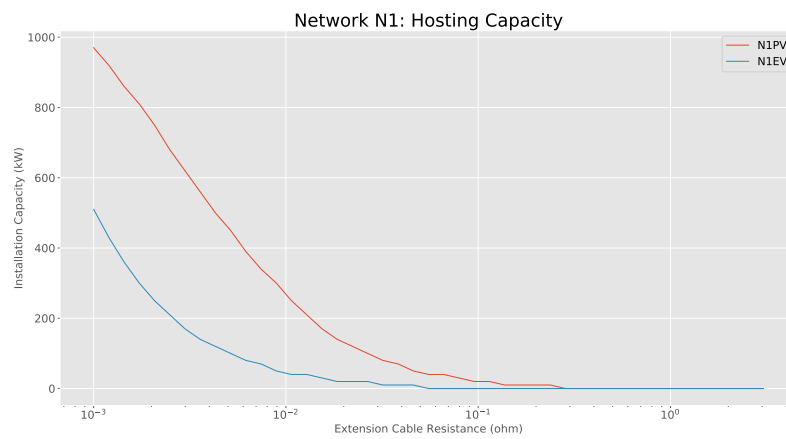


Figure 12.9: Hosting Capacity of Network N1

Figure 12.9 shows the hosting capacity of the independent PV, or EV charger systems. For the PV system, between a hosting capacity of 970 kW, and 340 kW, the reason for limiting is the reached voltage level limit at the PV system's feeder. Below 340 kW, the reason is the reached voltage drop limit on the feeder. For the EV charger system, the reason for limiting is the reached voltage drop limit on the feeder.

12.3.2 Network N2

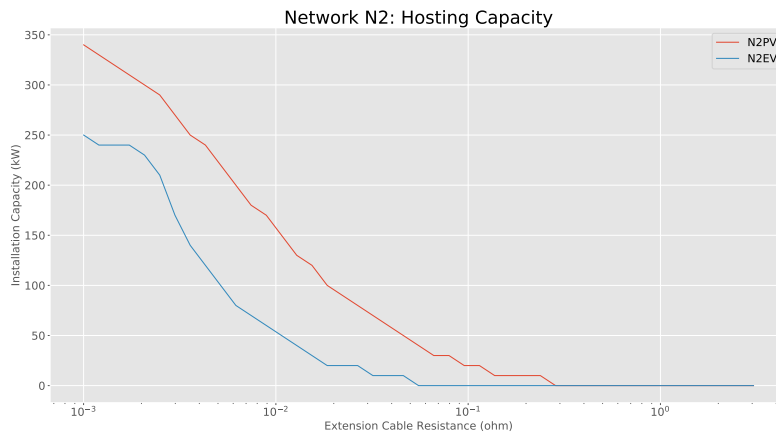


Figure 12.10: Hosting Capacity of Network N2

Figure 12.10 shows the hosting capacity of the independent PV, or EV charger systems. For the PV system, between a hosting capacity of 340 kW and 60 kW, the reason for limiting was the reached voltage levels at the PV system's feeder. Below a hosting capacity of 60 kW, the reason for limiting are both the voltage drop limit as the voltage level limit.

Finally, for the EV charger system, between a hosting capacity of 250 kW and 230 kW, the reason for limiting was the voltage unbalance at the EV charger system's feeder. Below 210 kW, the reason for limiting the hosting capacity was the reached voltage drop limit on the EV charger system's feeder.

12.3.3 Network N3

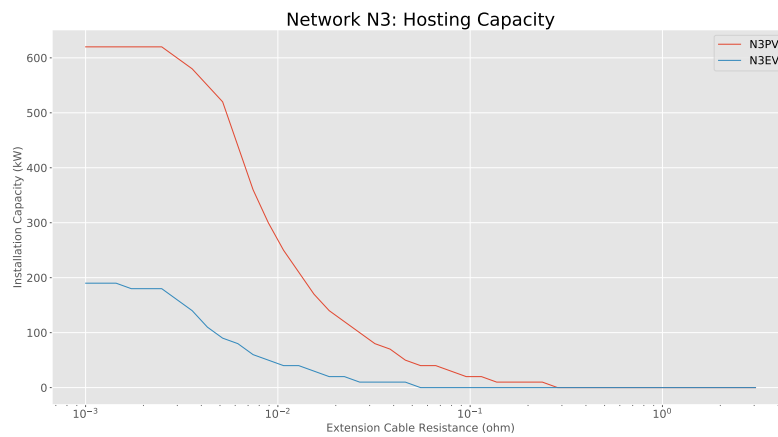


Figure 12.11: Hosting Capacity of Network N3

Figure 12.11 shows the hosting capacity of the independent PV, or EV charger systems. The figure of N3PV shows a straight line at the start of the figure. Here, the maximum iteration for raising P was reached. Between a capacity of 600 kW and 520 kW, the reason for limiting the hosting capacity is the reached voltage level limit. Below 520 kW, the reason was the reached voltage drop limit.

For the EV charger system, between a hosting capacity of 190 kW and 180 kW, the reason for limiting was the voltage unbalance at the EV charger system's feeder. Below a hosting capacity of 180 kW, the reason for limiting was the reached voltage drop limit on the system's feeder.

12.3.4 Network N4

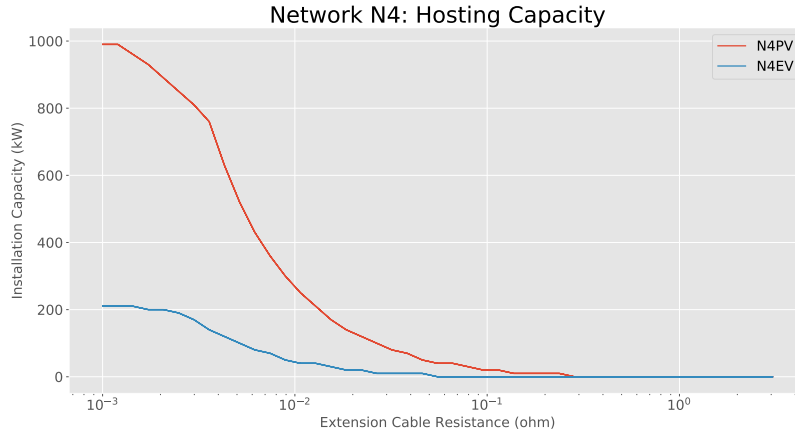


Figure 12.12: Hosting Capacity of Network N4

Figure 12.12 shows the hosting capacity of the independent PV, or EV charger systems. Similarly to N3PV, N4PV shows a straight line at the start of the graph, meaning that the maximum iteration was reached. Between a capacity of 960 kW and 760 kW, the reason for the hosting capacity was the reached voltage level at the main feeder. Below a capacity of 810 kW, the reason was the reached voltage drop limit on the system's feeder.

In N4EV, between a capacity of 210 kW and 190 kW, the reason for limiting the capacity was the unbalance limit at the system's feeder. Below a capacity of 190 kW, the reason for limiting was the voltage drop limit at the system's feeder.

12.4 Discussion of the Algorithm's Results

For low impedances, the hosting capacity of the PV system was mainly limited by the utility voltage. This is because the utility voltage in these analyzed networks was relatively high. For higher impedances, the voltage drop limit on the PV system's feeder was reached, before the total voltage drop between the grid and the PV system would lead to breaching the voltage level limit.

In all networks, with the exception of Network N1, for low impedances, voltage unbalance limits were reached, while calculating the hosting capacity of EV charger systems. The unbalanced voltage drop on the network's main feeder and EV charger system's feeder had become sufficiently high to reach the voltage unbalance limit at the EV charger system. However, for higher impedances, the voltage drop limit on the EV charger system's feeder was

reached sooner.

The reason for Network N1 not reaching voltage unbalance limits at low impedances is because the network impedance of Network N1 is already low. It would take a much lower EV system's feeder's impedance before the total voltage drop between the grid and the EV system would lead to a voltage unbalance sooner.

Essentially, another question that could be answered using this algorithm is the following. "At which cable impedance and installed capacity, of the PV or EV charger system, would the network be more likely to reach voltage drop limits, or voltage level and voltage unbalance limits?" An answer to this question could be very beneficial for the design of the PV or EV charger system. The system designer may be more inclined to design the system based on voltage drop limits. This is because reaching voltage drop limits does not necessarily risk the tripping or damaging of devices, whereas reaching the voltage unbalance and voltage level limits do.

Part IV

Discussion, Conclusion, Recommendations and Future Work

Chapter 13

Discussion

The operation of the hosting capacity algorithm was successful. Next to finding the hosting capacity, the outcome also provided answers with relation to the design of the PV or EV charger system. This is because the algorithm not only considered the voltage levels and unbalances in the network, but also the voltage drops as suggested by the IEC. This makes it different than other algorithms that calculate hosting capacity. Many studies seemed to have focused on the perspective of the grid operator [36] [37] [38] [39]. As the grid operator is responsible for the voltage levels and unbalances, other limits are omitted.

A great part of the hosting capacity algorithm were the scenarios. The fact that the modeling, behind the PV generation and EV charging subscenarios, were based and compared to real measurements, provided a stronger case for the final scenarios. In the algorithm, a choice of subscenarios was made, using the Scenario Maker. The goal of the Scenario Maker was to create the worst case situations for the calculation of the hosting capacity. This lead to a decision algorithm. Subscenarios of PV generation, EV charging, and network loading were chosen based on the highest expected voltage drop. This is advantageous since the voltage drop also considers the effect of reactive power. The worst case subscenario of EV charging was also based on the highest expected voltage unbalances.

The core model of the algorithm was based on power-flow equations. It was advantageous to build the model from the ground up, and finally create a dedicated code. It is believed that this was a big factor in limiting the time that it takes to calculate the voltage variations and unbalances.

The outcome of the hosting capacity also depends on the monitoring data. Monitoring data is useful for determining the worst case scenarios. This is because a lot of information about the daily load patterns are available. However, the device type and programming of the monitoring device should be considered. For calculating the slow voltage variations and unbalances, 10 minute averages of the active and reactive power demand is required. In

this case, 15 minute snippet measurements were provided by the monitoring devices. It is believed that the outcome of the algorithm was less accurate because of this reason. However, the operation of the hosting capacity algorithm could still be demonstrated.

Finally, the Scenario Maker was an unexpected part of the thesis project. The research questions focused much on the behaviour of different aspects that influence slow voltage variations and unbalances. Also, the creation of a model that calculated them was considered. However, later in the thesis, the importance of choosing relevant scenarios had come up, which had resulted into the Scenario Maker. The Scenario Maker has proven to be a constructive part of the algorithm, because it had resulted in more accessible results.

Chapter 14

Conclusion

In this thesis, an algorithm that calculates the hosting capacity of independent PV, or EV charger systems was created. This algorithm was used to calculate the hosting capacity for four different industrial and commercial LV networks, of which the monitoring data was provided by the company HyTEPS.

The hosting capacity is based on slow voltage variations and voltage unbalances. These aspects depend on the utility voltage as provided by the grid, the impedance of the network, and finally the current flow in the network.

In a network where a PV system is installed, the network may experience voltage raises due to a mismatch in power generation and loading. Furthermore, the PV generation may aggravate the current unbalances, and finally the voltage unbalances in the network. The generation of PV depends on the PV module's characteristics, the tilt, and the azimuth angle. Secondly, PV generation depends on the position of the sun relative to the module.

Additionally, a network, where an EV charger system is installed, may be subject to a voltage level decrease and voltage unbalances. This depends on the time of EV connection to the network, the time that it takes to charge a car, the maximum phase power of the cars and the charger, the amount of cars connected, and finally the three-phase charging capability of the cars and chargers.

Commercial and industrial loading typically show high loads during the weekdays, and low demand during the weekends. The weekend demand could limit the PV generation, because the voltage may increase too much. The weekday demand could limit the EV charging, because it contributes to the voltage drop in the network. Finally, the loads in the analyzed networks were mainly balanced. Therefore, it is not expected that three-phase PV generation would aggravate the current unbalances too much. However, EV charging may still create significant voltage unbalance due to single phase charging.

The behaviour of the PV and EV charger systems have been modelled. Subsequently the worst case subscenarios of the PV and EV charger systems were created. Finally, the worst case subscenarios for the network loading and utility voltage were drawn from the analyzed networks. These subscenarios were combined into two scenarios for the PV, and EV charger system, respectively. Then, the hosting capacity was calculated for a range of PV and EV charger system's impedances. This resulted into two figures for each of the networks, which are helpful for the design of the independent PV and EV charger systems.

Chapter 15

Recommendations and Future Work

The Scenario Maker is a large part of the algorithm. Therefore, improvements of the Scenario Maker could make a lot of difference in the outcome of the model. The Scenario maker could be improved by adding the element of time by (mis)matching the the exact behaviours of PV generation and the network loading, or EV charging and the network loading. However, trying to mismatch each daily pattern, especially when a lot of monitoring data is available, is likely very time consuming, and requires optimization.

The scenarios created by the Scenario Maker was based on the worst case situations. Alternatively, the Scenario Maker could be based on the most frequent PV generation or EV charger situations. For example, the Scenario Maker could be based on the most frequent network loading situations throughout the year. However, this alteration may require a risk/benefit analysis, considering the risk of the worst case scneario actually happening.

Finally, due to the variability of the models, if more information about the installed PV and EV charger system is known, it is possible to alter the PV generation and EV charging modelled inputs. For example, when the network can only expect three-phase EV charging, the worst case scenario will be different. Moreover, a difference in tilt or azimuth angle, of the PV system, will lead to a different worst case scenario as well.

Bibliography

- [1] NASA, “Climate change: How do we know?” [Online]. Available: <https://climate.nasa.gov/evidence/>
- [2] E. Comission, “Eu climate action.” [Online]. Available: https://ec.europa.eu/clima/citizens/eu_en
- [3] Rijksoverheid, “Financile ondersteuning elektrisch rijden,” 2019. [Online]. Available: <https://www.rvo.nl/onderwerpen/duurzaam-ondernemen/energie-en-milieu-innovaties/elektrisch-rijden/financi%C3%ABle-ondersteuning>
- [4] G. Kavlak, J. McNerney, and J. E. Trancik, “Evaluating the causes of cost reduction in photovoltaic modules,” *Energy Policy*, vol. 123, pp. 700 – 710, 2018. [Online]. Available: <http://www.sciencedirect.com/science/article/pii/S0301421518305196>
- [5] M. M. Haque and P. Wolfs, “A review of high pv penetrations in lv distribution networks: Present status, impacts and mitigation measures,” *Renewable and Sustainable Energy Reviews*, vol. 62, pp. 1195 – 1208, 2016. [Online]. Available: <http://www.sciencedirect.com/science/article/pii/S1364032116300429>
- [6] G. A. Putrus, P. Suwanapingkarl, D. Johnston, E. C. Bentley, and M. Narayana, “Impact of electric vehicles on power distribution networks,” in *2009 IEEE Vehicle Power and Propulsion Conference*, Sep. 2009, pp. 827–831.
- [7] P. Maheshwari, Y. Tambawala, H. S. V. S. K. Nunna, and S. Doolla, “A review on plug-in electric vehicles charging: Standards and impact on distribution system,” in *2014 IEEE International Conference on Power Electronics, Drives and Energy Systems (PEDES)*, Dec 2014, pp. 1–6.
- [8] F. D. Garcia, F. P. Marafo, W. A. d. Souza, and L. C. P. d. Silva, “Power metering: History and future trends,” in *2017 Ninth Annual IEEE Green Technologies Conference (GreenTech)*, March 2017, pp. 26–33.

- [9] Enexis, “Langzame spanningsvariatie: Wat is langzame spanningsvariatie?” [Online]. Available: <https://www.enexis.nl/zakelijk/-/media/documenten/spanningskwaliteit/langzame-spanningsvariatie.pdf?la=nl-nl&modified=20180123141428&hash=0AFE5B5AFF979BEE66924EAF4641F9BDD81C25E8>
- [10] P. to Phase, “Spanning bij langzame spanningsvariates.” [Online]. Available: https://phasetophase.nl/boek/boek_2.11.html#.11.3
- [11] E. I. Wiki, *Definition of voltage ranges: IEC voltage standards and recommendations.*, Schneider Electric, Oct. 2018. [Online]. Available: http://www.electrical-installation.org/enwiki/Definition_of_voltage_ranges
- [12] S. Electric, “Maximum voltage drop limit,” Electrical Installation Wiki, May 2018. [Online]. Available: http://www.electrical-installation.org/enwiki/Maximum_voltage_drop_limit
- [13] “Definitions of voltage unbalance,” *IEEE Power Engineering Review*, vol. 21, no. 5, pp. 49–51, May 2001.
- [14] M. Albadi, A. Al-Hinai, A. Al-Badi, M. Al Riyami, S. Al-Hinai, and R. Al Abri, “Unbalance in power systems: Case study,” *Proceedings of the IEEE International Conference on Industrial Technology*, vol. 2015, pp. 1407–1411, 06 2015.
- [15] A. C. . Markt, “Netcode electriciteit,” May 2016. [Online]. Available: <https://www.acm.nl/nl/publicaties/publicatie/14381/Netcode-Elektriciteit>
- [16] A. S. Masoum, P. S. Moses, M. A. S. Masoum, and A. Abu-Siada, “Impact of rooftop pv generation on distribution transformer and voltage profile of residential and commercial networks,” pp. 1–7, Jan 2012.
- [17] T. Aziz and N. Ketjoy, “Pv penetration limits in low voltage networks and voltage variations,” *IEEE Access*, vol. 5, pp. 16 784–16 792, 2017.
- [18] *WINAICO WSP-M6 Data Sheet*, Win Win Precision Technology Co. [Online]. Available: <https://www.zonnepanelen.net/nl/pdf/panels/datasheet-winaico-wsp-295m6-perc-zonnepaneel.pdf>
- [19] Y. D. Wijs, “Juli 2018: Recorddroog, recordzonnig en zeer warm,” Jul. 2018. [Online]. Available: <https://www.knmi.nl/nederland-nu/klimatologie/maand-en-seizoensoverzichten/2018/juli>
- [20] A. Huiskamp, “December 2018: Zeer zacht, aan de natte kant en de normale hoeveelheid zonneschijn,” Jan. 2019.

- [21] F. Corporation, “Technical data: Fluke 430 series ii three-phase power quality and energy analyzers,” 2016. [Online]. Available: https://dam-assets.fluke.com/s3fs-public/2643006_6112_ENG_E_W.PDF
- [22] J. C. Spoelstra, “Charging behaviour of dutch ev drivers,” Master’s thesis, Utrecht University, Jul. 2014. [Online]. Available: <https://www.rvo.nl/sites/default/files/2014/10/Master%20Thesis%20Charging%20behaviour%20of%20Dutch%20EV%20drivers.pdf>
- [23] E. E. Limited, “Electric vehicle charging behaviour study,” Mar. 2019. [Online]. Available: <http://www.element-energy.co.uk/wordpress/wp-content/uploads/2019/04/20190329-NG-EV-CHARGING-BEHAVIOUR-STUDY-FINAL-REPORT-V1-EXTERNAL.pdf>
- [24] EVBOX, “Check charging specifications,” 2019. [Online]. Available: <https://evbox.com/en/electric-cars/>
- [25] P. T. Phase, “Netten voor distributie van elektriciteit,” 2009-2017. [Online]. Available: https://phasetophase.nl/boek/boek_2_10.html#_10.2
- [26] I. Transformers, “Nl norm n15 transformatoren,” 2019. [Online]. Available: <https://www.ieotrafo.com/nl/transformatoren/nederlandse-norm-transformatoren/>
- [27] G. C. Mouli, P. Bauer, and M. Zeman, “System design for a solar powered electric vehicle charging station for workplaces,” *Applied Energy*, vol. 168, pp. 434–443, apr 2016.
- [28] KNMI, “Meteorological data portal,” Internet, 2019. [Online]. Available: <https://www.tudelft.nl/en/eemcs/the-faculty/departments/electrical-sustainable-energy/photovoltaic-materials-and-devices/dutch-pv-portal/data-portal/>
- [29] V. V. Ashok, C. Onwudinanti, G. R. C. Mouli, and P. Bauer, “Matching pv array output with residential load by optimisation of array orientation,” jun 2015.
- [30] V. Aggarwal, “What are the most efficient solar panels on the market? solar panel efficiency explained.” Jul. 2019. [Online]. Available: <https://news.energysage.com/what-are-the-most-efficient-solar-panels-on-the-market/>
- [31] C. Crowell, “Solar pv inverter buyers guide 2019: Faster installs, better serviceability and a focus on storage,” Mar. 2019. [Online]. Available: <https://solarbuildermag.com/news/solar-pv-inverter-buyers-guide-2019/2>

- [32] T. S. community, *scipy.optimize.fsolve*, SciPy.org, May 2014. [Online]. Available: <https://docs.scipy.org/doc/scipy-0.14.0/reference/generated/scipy.optimize.fsolve.html>
- [33] H. L. Nguyen, “Newton-raphson method in complex form [power system load flow analysis],” *IEEE Transactions on Power Systems*, vol. 12, no. 3, pp. 1355–1359, 1997.
- [34] *Installatiehandleiding Basis & Meterkast tot Omvormer*, Zonnepanelen discounter. [Online]. Available: <https://zonnepanelendiscounter.net/uploads/files/basis-handleiding-zonnepanelendiscounter.pdf>
- [35] Y.-K. Wu, J.-H. Lin, and H.-J. Lin, “Standards and guidelines for grid-connected photovoltaic generation systems: A review and comparison,” *IEEE Transactions on Industry Applications*, vol. 53, no. 4, pp. 3205–3216, jul 2017.
- [36] M. Cresta, F. M. Gatta, A. Geri, L. Landolfi, S. Lauria, M. Maccioni, M. Paulucci, and M. Pompili, “Prospective installation of EV charging points in a real LV network: Two case studies,” sep 2012.
- [37] A. Ballanti and L. F. Ochoa, “On the integrated PV hosting capacity of MV and LV distribution networks,” oct 2015.
- [38] F. Baccino, M. de Nigris, S. Massucco, and E. Tironi, “A methodology for evaluating PEVs hosting capacity margins in distribution grids,” jul 2012.
- [39] A. Dubey, S. Santoso, and A. Maitra, “Understanding photovoltaic hosting capacity of distribution circuits,” jul 2015.